Theoretical and Numerical Modeling of Nonlinear Electromechanics with applications to Biological Active Media

Alessio Gizzi[1], Christian Cherubini[1,2,*], Simonetta Filippi[1,2] and Anna Pandolfi[3]

[1] *Nonlinear Physics and Mathematical Modeling Laboratory, and*
[2] *International Center for Relativistic Astrophysics Network, I.C.R.A.Net,*
University Campus Bio-Medico of Rome, Via A. del Portillo 21, 00128 Rome, Italy.
[3] *Civil and Environmental Engineering Department*
Politecnico di Milano, Piazza Leonardo da Vinci 32, 20133 Milano, Italy.

Abstract. We present a general theoretical framework for the formulation of the nonlinear electromechanics of polymeric and biological active media. The approach developed here is based on the additive decomposition of the Helmholtz free energy in elastic and inelastic parts and on the multiplicative decomposition of the deformation gradient in passive and active parts. We describe a thermodynamically sound scenario that accounts for geometric and material nonlinearities. In view of numerical applications, we specialize the general approach to a particular material model accounting for the behavior of fiber reinforced tissues. Specifically, we use the model to solve via finite elements a uniaxial electromechanical problem dynamically activated by an electrophysiological stimulus. Implications for nonlinear solid mechanics and computational electrophysiology are finally discussed.

1 Introduction

Electro-elastic (EA) media are physical systems that are sensitive to the action of mechanical forces and electric fields. When immersed in electric fields, EA systems deform spontaneously, and, when deformed by mechanical forces, they cause a change in the original

*Corresponding author. *Email addresses:* `a.gizzi@unicampus.it` (A. Gizzi), `c.cherubini@unicampus.it` (C. Cherubini), `s.filippi@unicampus.it` (S. Filippi), `anna.pandolfi@polimi.it` (A. Pandolfi)

configuration of electrostatic or electrodynamic fields. The variation of the assigned configuration of the electric field lines triggered by the electromechanical coupling is called mechanic-electric feedback (MEF). Typically, in EA systems deformations may induce a change of the eventual initial isotropy of a body.

Historically, the most well known example of electro-elastic systems has been the piezoelectric crystal. In linearized kinematics, it can be proved that an isotropic dielectric immersed in an electric field develops polarization charges, inducing internal stresses proportional to the square of the electric field [37]. A similar dynamics characterizes piezoelectrics. The origin of the electromechanical coupling in piezoelectric materials stems from a phase transition that breaks the symmetry, and that leads also to a spontaneous polarization. By this spontaneous polarization there is a linear coupling between deformation and electric field [36, 44], so that MEF effects are enhanced. Piezoelectrics manifest also the reverse feedback: imposed deformations induce an internal electric field proportional to the magnitude of the deformations. A second important class of materials where MEF is of relevance are electro-active polymers (EAP), that typically exhibit changes in size or in shape when stimulated by an electric field [53]. Among the recent literature addressing this class of materials, it is worth to mention contributions concerning electro-visco elastic polymers [4, 5, 74], and proposing thermodynamic formulations for electro-active synthetic materials [46].

The MEF effect is observed also in materials that are in focus in the present study, i.e., biological media with contractile properties, such as the heart, the intestines, and several types of muscles. It is evident that biological systems undergo rather large deformations, therefore the underlying biophysical dynamics cannot be described accurately by means of the infinitesimal theory of elasticity. In particular, according to single cell and tissue specimen measurements, during a normal heart beat myocytes change their length up to 20% [50], i.e., in the typical range of finite deformations. According to the literature, the mechanical properties of muscles have been mainly investigated at the macroscopic scale via force-velocity relationships, following Hill's model [30]. The complexity of the electric fields and of the mechanics of the heart, however, requires to adopt a multiscale perspective, since the cardiac contraction connects the global mechanical properties observed at the organ scale [78] to the underlying subcellular dynamics [32].

The cardiac beating is the result of the propagation of electrical waves generated by the sequential excitation of neighboring cells, located along specialized conductive structures that provide the spreading of the electric signal into the whole heart [35, 49, 57, 66]. In turn, the excitation of a cardiac cell is induced by the variation of the electric potential across the cell membrane. Changes in the electric potential are related in a nonlinear manner to the transmembrane fluxes of various charged ions.

The basic features of the mechanical response of biological active tissues can be sufficiently well described by hyperelastic models, disregarding in first approximation more complicated effects related to viscosity, growth and remodeling. Since the '80s, several mathematical models of passive muscle and myocardium elasticity have been proposed, including isotropic, transversely isotropic and, more recently, orthotropic models [31,39].

The interest towards the modeling of the active behavior of deformable biological tissues has been growing progressively in the last decade. As one of the first contributions in this field, the response of muscle fibers to the activation-contraction coupling process has been studied in [59]. From the continuum mechanics point of view, the internal actin-myosin binding can be considered as a micro-structural alteration of the internal kinematic state of the muscle fiber, which leads to changes in the macroscopic behavior. Since the sliding of the myosin filaments occurs clearly in the direction of the fiber axis, the binding between actin and myosin filaments has been associated in general only to the change in the longitudinal size of the fiber, assuming that no variations take place in the cross-section of the fiber. The introduction of the active stress component in the formulation encompasses the key aspects related to the description of the subcellular electrophysiological dynamics of the tissue. In particular, the autoregulation of calcium inward and outward fluxes within a myocyte, accurately described in [15], can be related to activation and de-activation processes of actin and myosin proteins [29], and, by the way of extension, to the macroscopic tissue deformation.

As already mentioned, in order to account for the strong contraction induced by the electromechanical coupling, the behavior of active bio-materials must be described in terms of finite deformations, following the lines of relevant recent works, see, e.g., [25, 52, 62, 70, 71, 75, 76]. The standard approach for modeling bio-active tissues is based on a passive response expressed in terms of hyperelastic weakly compressible or incompressible materials, combined to an active response (or active stress) formulated in an independent way, in several cases as a phenomenological description of some inelastic action. As opposed to the concept of active stress, alternative approaches rely on the concept of active strain. An alternative formulation based on the multiplicative decomposition of the deformation gradient into active part and passive part have appeared recently in the cardiac literature [9, 10]. The formulation was based on several simplifying assumptions, which have been partially removed by other authors [3].

Apparently, the active stress and active strain approaches are in contrast, but since they aim at describing a unique phenomenon, they must be linked. A few examples in the literature have tried to establish a connection between the two approaches [25, 65]. Interestingly, by relying on a consistent thermodynamic framework, it is possible to prove that the two approaches are fully compatible and they can be seen as two different aspects of the same theory. In particular, here we propose a class of constitutive models for electro-active materials based on: (i) the multiplicative decomposition of the deformation gradient in passive and active parts; (ii) an additive decomposition of the underlying Helmholtz free energy density; (iii) the separation of the arguments between the different terms of the strain energy density. Our formulation adopts a fully thermodynamic approach, and is able to conciliate the contrasting concepts of active stress and active strain. In addition, in the present paper we describe a simplified class of anisotropic electromechanical active material models, in view of future numerical simulations of the behavior of muscles and heart.

The organization of the paper is as follows. In Section 2 we provide the general frame-

work of the coupled thermo-electromechanical problem, including time-dependent behaviors. In Section 3 we restrict our scope to isothermal electromechanical active media and derive general constitutive relationships by assuming a decoupled expression of the Helmholtz free energy density. In Section 4 we specialize the free energy density to a particular anisotropic model and analyze the constitutive behavior of the model in uniaxial and biaxial loading. Then we use the approach to solve via finite elements a uniaxial electromechanical problem dynamically activated by an electrophysiological stimulus. Conclusions and future perspectives are reported in Section 5.

2   Formulation of the problem

We recall the field equations that will be of relevance in the subsequent derivations. It is worth to mention that, unlike piezoelectrics, biological tissues behave as nonlinear electrical conductors, although mechanically they can be considered as deformable dielectrics. For this reason, electrodynamics can be characterized by the electric reaction-diffusion equation. Extensive discussions on electromechanics of continua can be found in the literature [13,16,43,47,58,70].

Linear and angular momentum balance

We refer to a body of mass density per unit volume ρ_0 undergoing a motion $x(X,t)$, where X are the coordinates in the material configuration, x are the coordinates in the spatial configuration, $F = \nabla_X x$ is the deformation gradient, belonging to the Lie group of invertible and orientation-preserving linear transformations in $\mathbb{R}^3$, and $C = F^T F$ is the Cauchy-Green deformation tensor. The volume and the boundary with outward normal N in the material configuration are denoted by B_0 and ∂B_0 respectively. Correspondingly, the volume and the boundary with outward normal n in the spatial configuration are denoted by B and ∂B respectively.

The volume change is measured by

$$\det F = J = \frac{\rho_0}{\rho}, \tag{2.1}$$

where ρ is the mass density per unit deformed volume. Relation (2.1) states the local form of the mass balance.

The local form of the linear momentum is:

$$\rho_0 \frac{dV}{dt} = \nabla_X \cdot P + \rho_0 B, \tag{2.2}$$

where B are the body forces per unit of mass, V is the material velocity, and P is the first Piola-Kirchhoff stress tensor. The angular momentum balance is satisfied through the symmetry of the product:

$$PF^T = FP^T,$$

and the boundary condition with the tractions T is expressed through the Cauchy's relation:

$$T = PN.$$

In practical applications, it is preferable to use the weak form of the linear momentum balance, which in the material configuration becomes [45, 60]

$$\int_{B_0} \rho_0 \frac{d\boldsymbol{V}}{dt} \cdot \tilde{\boldsymbol{\eta}} dV + \int_{B_0} \boldsymbol{P} : \nabla_X \tilde{\boldsymbol{\eta}} dV = \int_{\partial B_0} \boldsymbol{T} \cdot \tilde{\boldsymbol{\eta}} dS + \int_{B_0} \rho_0 \boldsymbol{B} \cdot \tilde{\boldsymbol{\eta}} dV,$$

where $\tilde{\boldsymbol{\eta}}$ denotes a vector test function.

Electrostatics

We introduce the spatial electric field $\boldsymbol{e}$ as the spatial gradient of the electric potential φ, i.e., $\boldsymbol{e} = -\nabla_x \varphi$. In the vacuum the electric induction (or electric displacement) $\boldsymbol{d}$ is proportional to the electric field $\boldsymbol{e}_0$ through the vacuum permittivity ϵ_0. Commonly, in the matter the electric induction $\boldsymbol{d}$ is expressed as the sum

$$\boldsymbol{d} = \epsilon_0 \boldsymbol{e} + \boldsymbol{\pi}, \tag{2.3}$$

where $\boldsymbol{\pi}$ is the density of the permanent and induced electric dipole moments in the material or polarization density. The polarization density $\boldsymbol{\pi}$ depends on the material and it must be provided through a constitutive relation. Although the form (2.3) is not the most general relationship, it will be used in the following to clarify the definition of the stresses. In the absence of electric free charges in the volume, in B the electric field $\boldsymbol{e}$ and the electric induction $\boldsymbol{d}$ must satisfy the equations of electrostatics

$$\nabla_x \times \boldsymbol{e} = \boldsymbol{0}, \qquad \nabla_x \cdot \boldsymbol{d} = 0, \tag{2.4}$$

where $\nabla_x \times$ denotes the spatial curl operator and $\nabla_x \cdot$ the spatial divergence operator. Let $\boldsymbol{E}$, $\boldsymbol{D}$, and $\boldsymbol{\Pi}$ denote the material electric field, the material electric induction, and the material polarization density, respectively. Assuming that the material electric field is the material gradient of the electric potential, i.e., $\boldsymbol{E} = -\nabla_X \varphi$, from the invariance of a scalar field we obtain

$$\boldsymbol{E} = -\frac{\partial \varphi}{\partial \boldsymbol{X}} = -\frac{\partial \varphi}{\partial \boldsymbol{x}} \frac{\partial \boldsymbol{x}}{\partial \boldsymbol{X}} = \boldsymbol{F}^T \boldsymbol{e},$$

while the electric induction and the polarization density transform as $\boldsymbol{D} = J\boldsymbol{F}^{-1}\boldsymbol{d}$ and $\boldsymbol{\Pi} = J\boldsymbol{F}^{-1}\boldsymbol{\pi}$. Such relations can be proved by a double application of the divergence theorem and accounting for the Nanson's relation, i.e., $\boldsymbol{n} ds = J\boldsymbol{F}^{-T}\boldsymbol{N} dS$ [13]. It follows that the material form of the equations of electrostatics (2.4), holding in B_0, are

$$\nabla_X \times \boldsymbol{E} = \boldsymbol{0}, \qquad \nabla_X \cdot \boldsymbol{D} = 0,$$

where $\nabla_X \times$ denotes the material curl operator and $\nabla_X \cdot$ the material divergence operator. Finally, the material electric induction is expressed as:

$$\boldsymbol{D} = J\epsilon_0 \boldsymbol{C}^{-1}\boldsymbol{E} + \boldsymbol{\Pi}, \tag{2.5}$$

where the first term accounts for the distortion of the electric field due to material deformation. Clearly, also the material polarization density needs to be described through a constitutive relationship.

Note that the equations of mechanics are decoupled from the equations of electrostatics. Coupling arises from the constitutive equations, that will be derived later from thermodynamical considerations.

Electric diffusion

In spatial description the electric diffusion equation (known as cable equation) is

$$C_E \frac{\partial \varphi}{\partial t} = -\nabla_x \cdot \boldsymbol{h}_E + I_E, \tag{2.6}$$

where $C_E = C_E(\boldsymbol{C})$ is the electric capacitance; $\boldsymbol{h}_E$ is the flux of electric charges, and $I_E = I_E(\varphi, \boldsymbol{C})$ is the total ionic transmembrane current. The symbol $\partial/\partial t$ denotes the time derivative in the spatial configuration. Eq. (2.6) holds in B, with Neumann boundary conditions

$$-[\![\boldsymbol{h}_E]\!] \cdot \boldsymbol{n} = \omega,$$

where ω is the charge density on the boundary in the spatial configuration and $[\![\boldsymbol{h}_E]\!]$ denotes the jump of $\boldsymbol{h}_E$ across the boundary. Incidentally, the basic electrophysiological processes of the cardiac tissue can be modeled through a reaction-diffusion equation of type (2.6) [1,64].

The material form of (2.6), holding in B_0, is

$$C_E \frac{d\varphi}{dt} = -\frac{1}{J}\nabla_X \cdot \boldsymbol{H}_E + I_E, \tag{2.7}$$

where the material electric flux derives as $\boldsymbol{H}_E = -J\boldsymbol{F}^{-1}\boldsymbol{h}_E$ and d/dt denotes the material time derivative. The corresponding boundary conditions are

$$-[\![\boldsymbol{H}_E]\!] \cdot \boldsymbol{N} = \Omega,$$

where Ω denotes the surface charge density in the material configuration.

The weak form of (2.6) is given by

$$\int_B C_E \frac{\partial \varphi}{\partial t} \eta \, dv + \int_B \boldsymbol{h}_E \cdot \nabla_x \eta \, dv = \int_{\partial B} \omega \eta \, ds + \int_B I_E \eta \, dv, \tag{2.8}$$

where η is a scalar test function. The weak form of (2.7) is obtained from Eq. (2.8) by using the Nanson's relation, i.e.,

$$\int_{B_0} J C_E \frac{\partial \varphi}{\partial t} \eta \, dV + \int_{B_0} \boldsymbol{H}_E \cdot \nabla_X \eta \, dV = \int_{\partial B_0} \Omega \eta \, dS + \int_{B_0} J I_E \eta \, dV.$$

A commonly used expression for the electric flux h_E assumes a linear dependence on the gradient of the electric potential, through a spatial second-order tensor of electric conductivities k_E, as

$$h_E = -k_E \nabla_x \varphi.$$

The corresponding material form expression for the electric flux H_E through a material second-order contravariant tensor of electric conductivities $K_E = F^{-1} k_E F^{-T}$ is

$$H_E = -J K_E \nabla_X \varphi.$$

A more general definition of the electric flux can be derived from constitutive assumptions, following the path drawn in the next section.

Energy balance and dissipation inequality

Within an extended thermo-electromechanical framework, the specific internal energy U of the system is contributed also by the electric energy, given by the electric field E times the material electric induction D [70]. Accounting for the mass (2.1) and the linear momentum (2.2) balance, the local form of the rate energy balance becomes

$$\dot{U} = P : \dot{F} + E \cdot \dot{D} + \rho_0 Q - \nabla_X \cdot H_T, \tag{2.9}$$

where $\dot{U}$ is the specific rate of the internal energy, Q the heat supply per unit mass, and H_T the material energy flux vector, consisting of heat flux and non-thermal energy flux. The second law of thermodynamics states the non negativeness of the total entropy production $\dot{\Gamma}$, in local form:

$$T\dot{\Gamma} = T\dot{N} - \rho_0 Q + T\nabla_X \cdot H_N \geq 0, \tag{2.10}$$

where $T > 0$ is the local absolute temperature, $\dot{N}$ the entropy rate per unit reference volume, and $H_N = H_T / T$ denotes the entropy flux [33]. Thus, the ratio Q/T defines the entropy supply. Relation (2.10) allows for the description of dissipative phenomena, such as heat flow and the development of irreversible deformations. Using (2.9), Eq. (2.10) can also be written as

$$T\dot{\Gamma} = T\dot{N} - \dot{U} + P : \dot{F} + E \cdot \dot{D} - \frac{1}{T} H_T \cdot \nabla_X T \geq 0. \tag{2.11}$$

Following [37], in the successive derivations we use a more convenient form of the equation of state that accounts explicitly for the electric field E, and introduce a modified internal energy $\tilde{U}$ as

$$\tilde{U} = U - D \cdot E, \tag{2.12}$$

that can be interpreted as an electric Gibbs free energy density in the material description. Using $\tilde{U}$, the local energy balance (2.9) becomes

$$\dot{\tilde{U}} = P : \dot{F} - D \cdot \dot{E} + \rho_0 Q - \nabla_X \cdot H_T,$$

and (2.11) becomes

$$T\dot{\Gamma} = T\dot{N} - \dot{U} + \boldsymbol{P} : \dot{\boldsymbol{F}} - \boldsymbol{D} \cdot \dot{\boldsymbol{E}} - \frac{1}{T} \boldsymbol{H}_T \cdot \nabla_X T \geq 0. \tag{2.13}$$

With a harmless abuse of notation, in the following we will use the symbol U instead of $\tilde{U}$ to denote the alternative expression of the internal energy.

3 Constitutive relations

Thermodynamically consistent constitutive equations are derived from thermodynamic potentials. According to [11] we assume that the local thermodynamic state of an infinitesimal neighborhood of the body B_0 is completely defined by the variables of state deformation gradient $\boldsymbol{F}$, entropy density N, electric field $\boldsymbol{E}$, and by a set of internal variables $\boldsymbol{Z}$. Internal variables must be included to consider the presence of dissipative phenomena, such as plasticity or damage, that might in turn lead to local increase of the temperature and to the activation of heat diffusion inside the body. Note that the nature of $\boldsymbol{Z}$ — scalar, vector, or tensor — must be specified according to the material model and the kind of dissipation to be described [41, 45]. It is also assumed that the caloric equation of state and the temperature equation, relating to the variables of state the internal energy U and the temperature T, respectively, are functions of the local state only, i.e.,

$$U = U(\boldsymbol{F}, N, \boldsymbol{E}, \boldsymbol{Z}), \qquad T = T(\boldsymbol{F}, N, \boldsymbol{E}, \boldsymbol{Z}), \tag{3.1}$$

see also recent extensions [47, 70]. Finally, the stress $\boldsymbol{P}$ is the sum of two terms, i.e., the equilibrium stress $\boldsymbol{P}^E$, depending on the variables of state only, and the viscous stress $\boldsymbol{P}^V$, depending on the state variables and on the rate of deformation $\dot{\boldsymbol{F}}$:

$$\boldsymbol{P} \equiv \boldsymbol{P}^E(\boldsymbol{F}, N, \boldsymbol{E}, \boldsymbol{X}) + \boldsymbol{P}^V(\boldsymbol{F}, N, \boldsymbol{E}, \boldsymbol{X}; \dot{\boldsymbol{F}}). \tag{3.2}$$

Taking the differential of $(3.1)_1$ we obtain

$$\dot{U} = \frac{\partial U}{\partial \boldsymbol{F}} : \dot{\boldsymbol{F}} + \frac{\partial U}{\partial N} \dot{N} + \frac{\partial U}{\partial \boldsymbol{E}} \cdot \dot{\boldsymbol{E}} - \boldsymbol{X} : \dot{\boldsymbol{Z}}, \tag{3.3}$$

where we introduce the thermodynamic forces conjugated to $\boldsymbol{Z}$:

$$\boldsymbol{X} \equiv - \frac{\partial U(\boldsymbol{F}, N, \boldsymbol{E}, \boldsymbol{Z})}{\partial \boldsymbol{Z}}.$$

Introducing (3.2-3.3) in (2.13) we obtain

$$T\dot{\Gamma} = \left(\boldsymbol{P}^E - \frac{\partial U}{\partial \boldsymbol{F}} \right) : \dot{\boldsymbol{F}} + \boldsymbol{P}^V : \dot{\boldsymbol{F}} + \left(T - \frac{\partial U}{\partial N} \right) \dot{N} - \left(\boldsymbol{D} + \frac{\partial U}{\partial \boldsymbol{E}} \right) \cdot \dot{\boldsymbol{E}} - \frac{1}{T} \boldsymbol{H}_T \cdot \mathrm{Grad} T + \boldsymbol{X} \cdot \dot{\boldsymbol{Z}}$$
$$\geq 0. \tag{3.4}$$

Recalling the proof in [11], since inequality (3.4) must hold for any admissible process it follows that

$$\boldsymbol{P}^E = \frac{\partial U(\boldsymbol{F},N,\boldsymbol{E},\boldsymbol{Z})}{\partial \boldsymbol{F}}, \qquad T = \frac{\partial U(\boldsymbol{F},N,\boldsymbol{E},\boldsymbol{Z})}{\partial N}, \qquad \boldsymbol{D} = -\frac{\partial U(\boldsymbol{F},N,\boldsymbol{E},\boldsymbol{Z})}{\partial \boldsymbol{E}},$$

leading to

$$T\dot{\Gamma} = \boldsymbol{P}^V : \dot{\boldsymbol{F}} - \frac{1}{T}\boldsymbol{H}_T \cdot \mathrm{Grad}\, T + \boldsymbol{X} \cdot \dot{\boldsymbol{Z}} \geq 0.$$

An alternative thermodynamic potential especially advantageous in constitutive theories is the material Helmholtz free energy density A, obtained through a Legendre transform as

$$A(\boldsymbol{F},T,\boldsymbol{E},\boldsymbol{Z}) = \inf_N \left\{ U(\boldsymbol{F},N,\boldsymbol{E},\boldsymbol{Z}) - TN \right\}. \tag{3.5}$$

The constitutive equations derived from (3.5) become:

$$\boldsymbol{P}^E = \frac{\partial A(\boldsymbol{F},T,\boldsymbol{E},\boldsymbol{Z})}{\partial \boldsymbol{F}}, \qquad N = \frac{\partial A(\boldsymbol{F},T,\boldsymbol{E},\boldsymbol{Z})}{\partial T}, \qquad \boldsymbol{D} = -\frac{\partial A(\boldsymbol{F},T,\boldsymbol{E},\boldsymbol{Z})}{\partial \boldsymbol{E}},$$

and the thermodynamic forces are defined as:

$$\boldsymbol{X} \equiv -\frac{\partial A(\boldsymbol{F},T,\boldsymbol{E},\boldsymbol{Z})}{\partial \boldsymbol{Z}}.$$

The framework is completed with the definition of the kinetic relations that enable the determination of $\boldsymbol{P}^V$, $\dot{\boldsymbol{Z}}$ and $\boldsymbol{H}_T$. An accurate discussion on this topic can be found in [33,77] where, in view of providing a variational characterization of the rate constitutive equations, the concept of a general dissipation potential is introduced.

   In the following we are interested in isothermal processes, therefore we simplify the expression of the Helmholtz free energy by dropping the explicit dependence on the internal variables and on the temperature. The resulting energy corresponds to the "electrical Gibbs free energy" illustrated in [70]. The relevant equations of state will reduce to:

$$\boldsymbol{P} = \boldsymbol{P}^E = \frac{\partial A(\boldsymbol{F},\boldsymbol{E})}{\partial \boldsymbol{F}}, \qquad \boldsymbol{D} = -\frac{\partial A(\boldsymbol{F},\boldsymbol{E})}{\partial \boldsymbol{E}}. \tag{3.6}$$

If the Helmholtz energy takes a complicated functional form, the equations of state will be in general nonlinear. In practical applications it will be necessary to linearize the equations of state in the neighborhood of a particular state characterized by $\boldsymbol{F},\boldsymbol{E}$. Linearization implies the definition of the hessian of the free energy, that will include the fourth order material elasticity tensor $\mathbb{D}$:

$$\mathbb{D} = \frac{\partial^2 A(\boldsymbol{F},\boldsymbol{E})}{\partial \boldsymbol{F} \partial \boldsymbol{F}}, \tag{3.7}$$

the third order electromechanical coupling tensor $\mathcal{S}$:

$$\mathcal{S} = -\frac{\partial^2 A(\boldsymbol{F},\boldsymbol{E})}{\partial \boldsymbol{F} \partial \boldsymbol{E}}, \tag{3.8}$$

and the second order electric tensor K:

$$K = -\frac{\partial^2 A(F,E)}{\partial E \partial E}. \tag{3.9}$$

A general Helmholtz potential for active electro-mechanics

In the description of the kinematics of an isothermal active electromechanical process we assume the multiplicative decomposition of the deformation gradient into elastic F^e and inelastic F^i parts as

$$F = F^e F^i, \qquad F^e = F F^{i^{-1}}. \tag{3.10}$$

The elastic part of the deformation gradient is related to the passive response of the material, while the inelastic part is introduced to describe the geometrical changes of the initial configuration induced by phenomena other than elasticity. In the present discussion, the inelastic deformation F^i must provide the active effects of the electric field on unconstrained portions of the material, therefore in general it will be a function of E, or on the electric potential φ. Assumption (3.10) introduces an ideal intermediate non compatible configuration where all the inelastic phenomena take place without inducing a stress state in the continuum. The compatibility requirement will relax the body from the intermediate configuration to the final deformed configuration, where equilibrium and compatibility conditions are fully satisfied.

The multiplicative decomposition of the deformation gradient is a convenient mathematical representation of the change of configuration of a system undergoing multiphysics processes in large deformations [14]. The formal introduction in nonlinear continuum mechanics of the multiplicative decomposition can be attributed to [69] in the case of thermoelasticity, and to [38] in the case of phenomenological elastoplasticity. More recently, the approach has seen successful applications in biomechanics to model growth [63] and electromechanical interactions [3,9,48].

Within the model of the multiplicative decomposition, the Helmholtz free energy can be split conveniently into two — or more — parts, and one part only can be considered as a function of the elastic strain by assuming a separation of the arguments of the single parts. The additive split of the free energy is appealing because the function can be chosen among the well-known strain energy functions for finite-strain elasticity. In the present case, the main motivation for adopting the free energy splitting and the argument separation is the need to achieve the physical distinction between passive and active behaviors of the material.

We are seeking a particular form of the material Helmholtz free energy able to provide the constitutive relations for active electromechanical problems. To this aim, we assume an additive decomposition of the free energy density in two distinct contributions as

$$A(F,F^e,E) = A^e(F^e) + A^i(F,E), \tag{3.11}$$

where we state explicitly the dependence on F^e of the free energy density. The term A^e in (3.11) represents the classical strain energy density of hyperelastic materials and is

assumed to be dependent only on the elastic part of the deformation gradient F^e. Any choice of hyperelastic strain energy functions is acceptable, according to the passive behavior of the material observed in experiments. The term A^i in (3.11) is an inelastic free energy density that accounts for the electric field and for all its effects, including inelastic deformations. We observe that the definition (3.11) does not reduce the electromechanical coupling to a purely geometrical effect, as it would happen if A^i were assumed to be a function of the sole electric field E, i.e., when it represents the electric energy density of the system. The full material coupling is implied by the inelastic free energy, dependent on both F and E.

Note that the additive decomposition of the Helmholtz free energy into elastic and inelastic parts accompanied by the multiplicative decomposition of the deformation gradient is typical of many constitutive theories in finite kinematics, see, e.g., [40,54–56], and it has been proved to be particularly efficient in numerical applications.

From assumptions (3.10)-(3.11), it follows that the equilibrium stress P decomposes into the sum of two terms

$$P = \frac{\partial A^e(F^e)}{\partial F} + \frac{\partial A^i(F,E)}{\partial F} = P^p + P^a. \tag{3.12}$$

We call the two terms passive stress P^p and active stress P^a respectively. The passive stress is defined as:

$$P^p = \frac{\partial A^e(F^e)}{\partial F^e} \frac{\partial F^e}{\partial F} = P^e F^{i-T}.$$

The stress P^p derives from the strain energy density A^e, which in the intermediate configuration defines the equilibrium stress P^e, work-conjugate to F^e. The elastic stress P^e is pulled-back to the reference configuration through the inverse inelastic deformation gradient F^{i-1}.

The active stress P^a is originated by the inelastic part A^i of the free energy and, as it will shown later, it is strictly related to the Maxwell stress associated to the presence of an electric field, cf. [70] for the case of dielectric elastomers.

The features of the model can be highlighted by stating explicitly the dependence of the inelastic free energy on the inelastic deformations induced by the electric field $F^i(E)$ as

$$A(F,F^e,E) = A^e(F^e) + A^i(F,F^i(E),E). \tag{3.13}$$

This allows to write the electric induction (3.6) as

$$D = -\frac{\partial A^i(F,F^i(E),E)}{\partial E} - \frac{\partial A^i(F,F^i(E),E)}{\partial F^i} \frac{\partial F^i(E)}{\partial E}. \tag{3.14}$$

The first term in (3.14) accounts for the electric induction in the absence of electric distortions carried by the material, i.e., the one observed in the vacuum. The second term accounts for the effects due to the presence of the material through the electric distortions F^i, therefore it must be related to the material polarization Π. In particular, if we account

for the common definition of the electric induction (2.5), it follows from (3.14) that the inelastic part of the free energy density must be of the form

$$A^i(\boldsymbol{F},\boldsymbol{F}^i(\boldsymbol{E}),\boldsymbol{E}) = A^E(\boldsymbol{F},\boldsymbol{E}) + A^{\Pi}(\boldsymbol{F},\boldsymbol{F}^i(\boldsymbol{E})), \tag{3.15}$$

where

$$A^E(\boldsymbol{F},\boldsymbol{E}) = -\frac{1}{2}\epsilon_0 J \boldsymbol{E}\boldsymbol{F}^{-1}\cdot\boldsymbol{F}^{-T}\boldsymbol{E} = -\frac{1}{2}\epsilon_0 J \boldsymbol{e}\cdot\boldsymbol{e} \tag{3.16}$$

would represent the electric energy density in absence of matter, i.e., when the electric field $\boldsymbol{E}$ is assumed to be the electric field in vacuum $\boldsymbol{E}_0$. If the matter is present, this term must account also for the deformation of the medium and therefore cannot represent the vacuum electric energy anymore, despite the presence of ϵ_0. The term $A^{\Pi}(\boldsymbol{F},\boldsymbol{F}^i(\boldsymbol{E}))$ in (3.15) accounts for the material interaction of the electric field with the dielectric and will be made explicit upon the definition of $\boldsymbol{F}^i$.

The material active stress $\boldsymbol{P}^a$ defined in (3.12) takes the form

$$\boldsymbol{P}^a = \frac{\partial A^E(\boldsymbol{F},\boldsymbol{E})}{\partial \boldsymbol{F}} + \frac{\partial A^{\Pi}(\boldsymbol{F},\boldsymbol{F}^i(\boldsymbol{E}))}{\partial \boldsymbol{F}},$$

where

$$\boldsymbol{P}_0^M \equiv \frac{\partial A^E(\boldsymbol{F},\boldsymbol{E})}{\partial \boldsymbol{F}} = \epsilon_0 J \left[\boldsymbol{E}\boldsymbol{F}^{-1}\otimes\boldsymbol{F}^{-T}\boldsymbol{E} - \frac{1}{2}\left(\boldsymbol{E}\boldsymbol{F}^{-1}\cdot\boldsymbol{F}^{-T}\boldsymbol{E} \right)\boldsymbol{I} \right]\boldsymbol{F}^{-T}$$

is the material counterpart of the Maxwell stress in the vacuum. In fact, using the Piola relation between the Cauchy stress and the first Piola-Kirchhoff stress, we obtain:

$$\boldsymbol{\sigma}_0^M = J^{-1}\boldsymbol{P}_0^M\boldsymbol{F}^T = \epsilon_0 \left[\boldsymbol{e}\otimes\boldsymbol{e} - \frac{1}{2}(\boldsymbol{e}\cdot\boldsymbol{e})\boldsymbol{I} \right],$$

which is the contribution for the vacuum derived by Maxwell [37]. Note that several definition of the Maxwell stress are possible and used in the literature [44,70]. Additionally, the material polarization density Π in (2.5) derives as

$$\Pi = -\frac{\partial A^{\Pi}(\boldsymbol{F},\boldsymbol{F}^i(\boldsymbol{E}))}{\partial \boldsymbol{F}^i}\frac{\partial \boldsymbol{F}^i(\boldsymbol{E})}{\partial \boldsymbol{E}}.$$

Note that the additive form of the free energy will transfer also to the Hessian (3.7-3.9) as

$$\mathbb{D} = \boldsymbol{F}^{i-1}\frac{\partial^2 A^e(\boldsymbol{F}^e)}{\partial \boldsymbol{F}^e \partial \boldsymbol{F}^e}\boldsymbol{F}^{i-T} + \frac{\partial^2 A^E(\boldsymbol{F},\boldsymbol{E})}{\partial \boldsymbol{F}\partial \boldsymbol{F}} + \frac{\partial^2 A^{\Pi}(\boldsymbol{F},\boldsymbol{F}^i(\boldsymbol{E}))}{\partial \boldsymbol{F}\partial \boldsymbol{F}},$$

$$\mathbb{K} = \epsilon_0 J \boldsymbol{C}^{-1} - \frac{\partial \boldsymbol{F}^i(\boldsymbol{E})}{\partial \boldsymbol{E}}\frac{\partial^2 A^{\Pi}(\boldsymbol{F},\boldsymbol{F}^i(\boldsymbol{E}))}{\partial \boldsymbol{F}^i \partial \boldsymbol{F}^i}\frac{\partial \boldsymbol{F}^i(\boldsymbol{E})}{\partial \boldsymbol{E}},$$

$$\mathbb{S} = -\frac{\partial^2 A^E(\boldsymbol{F},\boldsymbol{E})}{\partial \boldsymbol{F}\partial \boldsymbol{E}} - \frac{\partial^2 A^{\Pi}(\boldsymbol{F},\boldsymbol{F}^i(\boldsymbol{E}))}{\partial \boldsymbol{F}\partial \boldsymbol{F}^i}\frac{\partial \boldsymbol{F}^i(\boldsymbol{E})}{\partial \boldsymbol{E}}.$$

Under particular conditions, the energy A^{Π} can be taken dependent on the inelastic deformations $\boldsymbol{F}^i(\boldsymbol{E})$ only, i.e., $A^{\Pi}\!=\!A^{\Pi}(\boldsymbol{F}^i(\boldsymbol{E}))$. In this case, the stress and the energy Hessian reduce to

$$\boldsymbol{P}\!=\!\frac{\partial A^e(\boldsymbol{F}^e)}{\partial \boldsymbol{F}^e}\boldsymbol{F}^{i-T}\!+\!\boldsymbol{P}_0^M,$$

$$\mathbb{D}\!=\!\boldsymbol{F}^{i-1}\frac{\partial^2 A^e(\boldsymbol{F}^e)}{\partial \boldsymbol{F}^e \partial \boldsymbol{F}^e}\boldsymbol{F}^{i-T}\!+\!\frac{\partial^2 A^E(\boldsymbol{F},\boldsymbol{E})}{\partial \boldsymbol{F} \partial \boldsymbol{F}},$$

$$\mathcal{S}\!=\!-\frac{\partial^2 A^E(\boldsymbol{F},\boldsymbol{E})}{\partial \boldsymbol{F} \partial \boldsymbol{E}}.$$

The latter assumption leads to constitutive models similar to the ones discussed in [70] for ideal dielectric elastomers, except for the presence of the inelastic deformation $\boldsymbol{F}^i$. In these models, the deformation gradient and the electric field contribute to the free energy in independent ways and the electromechanical coupling is reduced to a purely geometric effect. As matter of fact, in ideal non-active dielectric elastomers (for which $\boldsymbol{F}^i = \boldsymbol{I}$), characterized by isotropy, the effect of the electric field can be described by a single material constant which is the permittivity ϵ of the material, which must replace ϵ_0 in (3.16). Evidently, the use of such models is restricted to isotropic materials.

Additionally, if the inelastic free energy density A^i is chosen to be null, the active electromechanical model reduces to a purely elastic model with kinematic constraints, introduced through the decomposition (3.10). The dependence on the electric field is enforced through $\boldsymbol{F}^i(\boldsymbol{E})$, but the coupling between electricity and mechanics is obtained in a phenomenological way [3,9,10,48]. The thermodynamical aspects of the electromechanical coupling are not considered. This choice can be convenient when experimental data are not sufficient to calibrate sophisticated material modes, or when it can be interesting to deal with a material able to develop inelastic deformations with no increase of internal energy.

The definition of the passive behavior through the strain energy density is not the main goal of this study. Accurate models for the description of the behavior of biological tissues are available in the literature, e.g., [9,24,27,31,34] and they can be applied to the present framework according to the application at the hand. Here we focus on the form of A^i, which must be able to describe the experimentally observed coupling between electricity and mechanics. A suitable choice of A^i must be associated to the expression of $\boldsymbol{F}^i$. As long as the inelastic deformation gradient is able to describe the coupling, the expression of A^i can be chosen as simple as possible.

In choosing the particular expression of $\boldsymbol{F}^i$ it is important to consider the characteristics of the material, including the underlying microstructure. For isotropic materials, a simple way to model the inelastic deformations consists in introducing a volumetric deformation and an enhanced stretch in the direction of the electric field, or

$$\boldsymbol{F}^i\!=\!(1\!+\!\gamma_{\mathrm{vol}})\boldsymbol{I}\!+\!\gamma_{\mathrm{dev}}\boldsymbol{E}\otimes\boldsymbol{E},$$

where γ_{vol} is a dimensionless parameter and γ_{dev} is a parameter with the dimensions of $|\boldsymbol{E}|^{-2}$, possibly dependent on the electric field intensity $|\boldsymbol{E}|$. In simple cases, γ_{vol} and γ_{dev}

can be assumed to be constant. Obviously, the expression of $\boldsymbol{F}^i$ in the case of anisotropic materials would be more general. For example, we can adopt

$$\boldsymbol{F}^i = \boldsymbol{F}^i(|\boldsymbol{E}|, \gamma^{(k)}, \boldsymbol{E} \otimes \boldsymbol{E}),$$

where (k) spans over the principal directions of anisotropy. When referred to the principal anisotropy directions $\boldsymbol{a}^{(k)}$, $\boldsymbol{F}^i$ can be described as:

$$\boldsymbol{F}^i(|\boldsymbol{E}|, \gamma^{(k)}, \boldsymbol{a}^{(k)}) = \boldsymbol{I} + \mathbb{F}(|\boldsymbol{E}|, \gamma^{(k)}) \boldsymbol{E} \otimes \boldsymbol{E},$$

where, for example, we can set:

$$\mathbb{F}(|\boldsymbol{E}|, \gamma^{(k)}) = \sum_{(k)} \left[\gamma_{\text{vol}}^{(k)} \mathbb{I} + \gamma_{\text{dev}}^{(k)} \mathbb{N}^{(k)} \right], \quad \mathbb{N}^{(k)} = \boldsymbol{a}^{(k)} \otimes \boldsymbol{a}^{(k)} \otimes \boldsymbol{a}^{(k)} \otimes \boldsymbol{a}^{(k)}, \tag{3.17}$$

with $(\mathbb{I})_{IJKL} = \delta_{IK}\delta_{JL}$ being the unit fourth order tensor. For transversally isotropic materials with the unique preferential direction $\boldsymbol{a}$, expression (3.17) reduces to

$$\mathbb{F}(|\boldsymbol{E}|, \gamma) = \gamma_{\text{vol}} \mathbb{I} + \gamma_{\text{dev}} \mathbb{N}. \tag{3.18}$$

In particular, according to (3.18), $\boldsymbol{F}^i$ becomes

$$\boldsymbol{F}^i = \left(1 + \gamma_{\text{vol}}|\boldsymbol{E}|^2\right) \boldsymbol{I} + \gamma_{\text{dev}}(\boldsymbol{E} \cdot \boldsymbol{a})^2 \boldsymbol{a} \otimes \boldsymbol{a}.$$

4   Numerical applications

The described framework is here applied to biological active tissues. In our numerical calculations we specialize the free energy density expression as described in the following section.

Electromechanics

We start by introducing a few simplifying assumptions. We restrict our attention to isothermal processes and assume A^e to be dependent only on the elastic deformation gradient $\boldsymbol{F}^e$. Additionally, we introduce the exact decomposition of $\boldsymbol{F}^e$ in volumetric and isochoric parts [67] as

$$\boldsymbol{F}^e = J^{e1/3} \overline{\boldsymbol{F}}^e,$$

where we denote $J^e = \det \boldsymbol{F}^e$. Material frame indifference requires the dependence on $\boldsymbol{F}^e$ through the modified Cauchy-Green deformation tensor $\overline{\boldsymbol{C}}^e = \overline{\boldsymbol{F}}^{eT} \overline{\boldsymbol{F}}^e$. For the description of the isotropic behavior, A^e is considered a function of the invariants $\overline{I}_1^e$ and $\overline{I}_2^e$

$$\overline{I}_1^e = \overline{\boldsymbol{C}}^e : \boldsymbol{I}, \qquad \overline{I}_2^e = \frac{1}{2} \left[\left(\text{tr}\overline{\boldsymbol{C}}^e \right)^2 - \text{tr}\left(\overline{\boldsymbol{C}}^{e2} \right) \right].$$

We include anisotropy through a unique structure tensor $\boldsymbol{G}$, which, in the case of a preferential direction $\boldsymbol{n}$ provided by the mean local orientation of a set of fibers, i.e., $\boldsymbol{G}=\boldsymbol{n}\otimes\boldsymbol{n}$. In general, anisotropy will characterize both the elastic and inelastic parts of the free energy density:

$$A(\boldsymbol{C},\boldsymbol{E},\boldsymbol{G})=A^e(\boldsymbol{C}^e,\boldsymbol{G})+A^i(\boldsymbol{C},\boldsymbol{E},\boldsymbol{G}).$$

The expressions of the elastic Helmholtz free energy density is written by considering an isotropic matrix obeying to a Mooney-Rivlin like material with embedded fibers along a preferential orientation. The elastic part is taken of the form:

$$A^e(\boldsymbol{C}^e,\boldsymbol{G})=W_{\text{vol}}(J^e)+W_{\text{iso}}(\overline{I}^e_1,\overline{I}^e_2)+W_{\text{fiber}}(\overline{\boldsymbol{C}}^e,\boldsymbol{G}),$$

where

$$W_{\text{vol}}(J^e)=\frac{1}{4}K\left(J^{e2}-1-2\log J^e\right); \tag{4.1}$$

$$W_{\text{iso}}(\overline{I}^e_1,\overline{I}^e_2)=\frac{1}{2}\left[\mu_1\left(\overline{I}^e_1-3\right)+\mu_2\left(\overline{I}^e_2-3\right)\right], \tag{4.2}$$

$$W_{\text{fiber}}(\overline{\boldsymbol{C}}^e,\boldsymbol{G})=\frac{1}{2}\frac{K_g}{k}\left[\exp k\left(\overline{I}^e_4-1\right)^2-1\right]. \tag{4.3}$$

In the previous relations, K is a stiffness parameter related to the bulk modulus, $\mu=\mu_1+\mu_2$ is a stiffness parameter related to the shear modulus, K_g is the stiffness of the fibers and k a dimensionless parameter that affects the fiber rigidity. The pseudo-invariant $\overline{I}^e_4$ is defined as [68]

$$\overline{I}^e_4=\overline{\boldsymbol{C}}^e:\boldsymbol{G}.$$

The use of the multiplicative decomposition of the deformation gradient into volumetric and isochoric parts, accompanied by the split of the strain energy density in volumetric and isochoric parts, has received recently some criticism [28]. In fact, a volumetric energy function of the sole volumetric deformation leads to a spherical stress, rather unrealistic in an anisotropic material. In [28] it has been suggested to adopt a volumetric strain energy density dependent also on the anisotropic pseudo invariants. In the present work, though, we decide to use the standard volumetric-isochoric decomposition used for isotropic materials for two reasons: (i) the model has been developed for nearly incompressible materials, and the volumetric strain energy is included to penalize the volumetric changes; (ii) the model not necessarily applies to anisotropic materials but also to isotropic materials.

Accounting for (3.15-3.16), the inelastic part of the Helmholtz free energy is taken of the form

$$A^i(\boldsymbol{C}(\boldsymbol{E}),\boldsymbol{E},\boldsymbol{G})=-\frac{1}{2}\epsilon_0 J\boldsymbol{E}\boldsymbol{F}^{-1}\cdot[\boldsymbol{I}+\chi(\boldsymbol{C}(\boldsymbol{E}),\boldsymbol{G})]\boldsymbol{F}^{-T}\boldsymbol{E},$$

where the susceptibility tensor χ is taken to be linear in $\boldsymbol{C}(\boldsymbol{E})$:

$$\chi(\boldsymbol{C}(\boldsymbol{E}),\boldsymbol{G})=\chi_0(\boldsymbol{G})+\mathbb{H}(\boldsymbol{G}):(\boldsymbol{C}(\boldsymbol{E})-\boldsymbol{I}). \tag{4.4}$$

We recall that, in virtue of (3.10), the Green-Cauchy tensor $C(E)$ is given by

$$C(E) = F^i(E)^T C^e F^i(E).$$

Let us assume a particular form of (4.4), where we describe the rank-two tensor χ_0 and the rank-four tensor $\mathbb{H}$ in terms of four constants χ_{iso}, χ_{fiber}, χ_{iso}^C and χ_{fiber}^C:

$$\chi_0(G) = \chi_{\text{iso}} I + \chi_{\text{fiber}} G, \qquad \mathbb{H}(G) = \chi_{\text{iso}}^C I \otimes I + \chi_{\text{fiber}}^C G \otimes G.$$

This allows to write (4.4) as

$$\chi(C,G) = \left[\chi_{\text{iso}} + \chi_{\text{iso}}^C (I_1(E) - 3) \right] I + \left[\chi_{\text{fiber}} + \chi_{\text{fiber}}^C (I_4(E) - 1) \right] G. \qquad (4.5)$$

The deformability is accounted for through the two invariants I_1, I_4 of the total right Cauchy-Green deformation tensor $C(E)$:

$$I_1(E) = C(E) : I, \qquad I_4(E) = C(E) : G.$$

In the proposed model, we introduce nine material constants: K, μ_1, μ_2, K_g, k, χ_{iso}, χ_{fiber}, χ_{iso}^C, and χ_{fiber}^C. The expression of the active and passive stresses is reported in the Appendix A.

4.1 Numerical examples

We test the response of the proposed material model under standard uniaxial, biaxial and shear loadings, reproducing the conditions of standard mechanical tests for biological tissues. The material constants adopted in the numerical examples have been selected in order to cover the range of stresses and deformations documented in the literature [2,26], and are collected in Table 1. The numerical tests are performed considering four different orientations of the fibers with respect to the direction of loading, i.e., 0^0, 30^0, 60^0 and 90^0. We report the results in terms of elastic Cauchy stress and Hencky strain.

Table 1: Anisotropic electro-mechanical parameters used in the examples of applications of the active electromechanical material model here described.

K	μ	μ_1	K_g	k	χ_{iso}	χ_{fiber}	χ_{iso}^C	χ_{fiber}^C	γ_{vol}	γ_{dev}
[kPa]	[kPa]	[kPa]	[kPa]	-	-	-	-	-	-	-
100	6	1	10	20	1	5	3	12	-0.0001	-0.0002

Passive response

We begin by evaluating the passive response for uniaxial, biaxial and shear response, keeping the direction 1 stress free. In the uniaxial tests we apply the stretch λ_3 and set the stress free in the direction 2, see Fig. 1(a). In the shear tests we apply a shear deformation γ_{32}, see Fig. 1(b). In the biaxial tests we apply $\lambda_2/\lambda_3 = 0.75$, see Fig. 1(c).

(a) Uniaxial   (b) Shear   (c) Biaxial
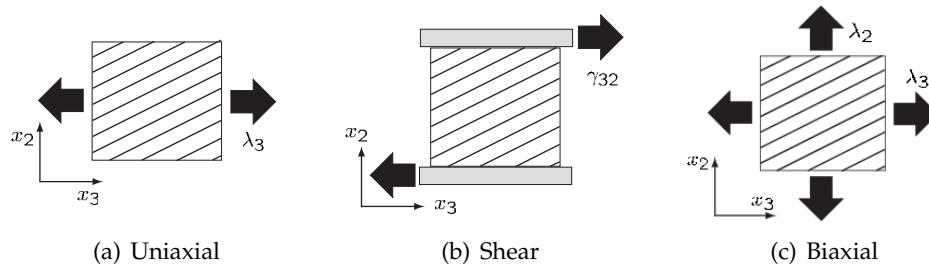
Figure 1: Schematic of the passive loading conditions for uniaxial, shear and biaxial tests. Direction 1, normal to the plane of the figure, is always stress free. For uniaxial and biaxial loading, the imposed stretch is in direction 3. Direction 2 is blocked for the shear case and stretched for the biaxial case with $\lambda_2/\lambda_3 = 0.75$. The fiber inclination varies between $0°$ and $90°$.

(a) Uniaxial   (b) Shear

(c) Biaxial   (d) Biaxial Transversal
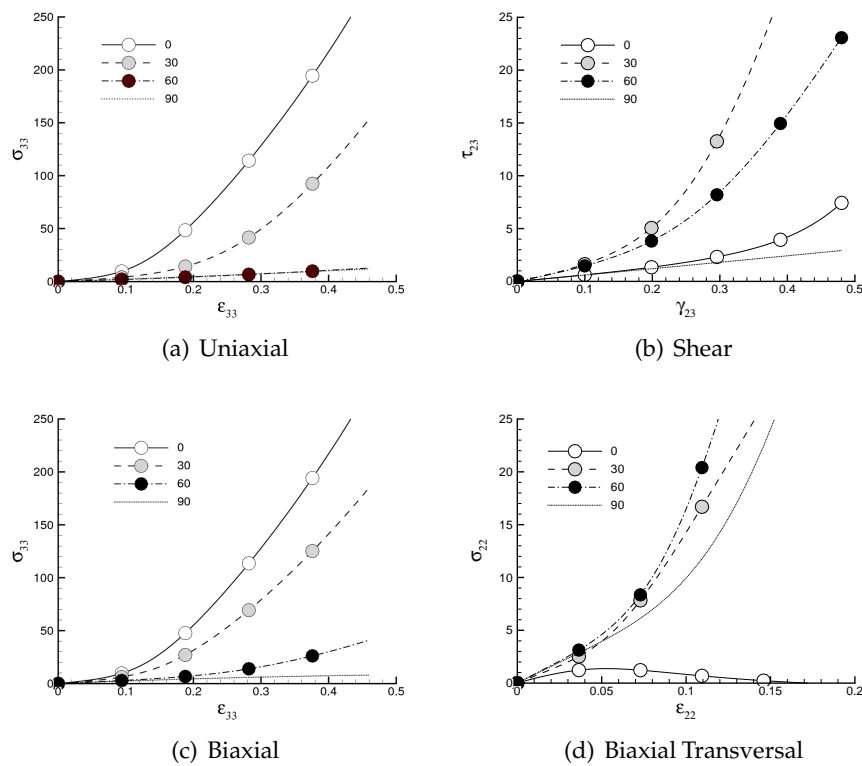
Figure 2: Passive response of the model under uniaxial, shear and biaxial loading, for different inclinations of the fibers with respect to the loading direction. Stresses in kPa.

The passive responses are shown in Fig. 2. In the uniaxial case, the stress decreases with the increase of the fiber inclination, and the contribution of the fiber to the stress drops to zero for fibers inclined more than $60°$, see Fig. 2(a).

For the shear loading, the cases where the fibers are parallel and orthogonal to the loading are characterized by a relatively small stress, clearly due to the isotropic part of

(a) Sensitivity on K_g (b) Sensitivity on k
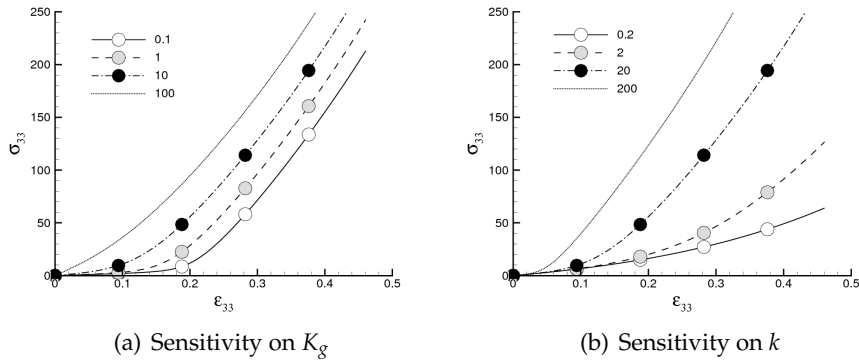
Figure 3: Passive response of the model under uniaxial loading for different values of the fiber stiffness parameters. (a) Sensitivity on K_g in the range 0.1-100 kPa for k=20. (b) Sensitivity on k, in the range 0.2-200, for $K_g = 10$ kPa. Stresses in kPa.

the strain energy, since both configurations are not prone to activate the fiber reinforcement. Because of the particular shear deformation applied, the case with fibers inclined $30°$ produces a response stiffer than the case with fibers inclined $60°$, see Fig. 2(b). These results are in close agreement with data reported by Dokos et al. [12].

In the biaxial configuration, the response in the direction of the applied stretch shows a small difference with respect to the uniaxial case, except for the fibers inclined $30°$ or $60°$, where the constraint in the direction 2 increases the stiffness of the response, see Fig. 2(c). The transversal stress for the biaxial case is about 10 times softer than the one in direction of the stretch, see Fig. 2(d). The stress is almost zero when fibers are aligned in the transversal direction. For fibers inclined $30°$, the stress is characterized by initial stiffening and final reduction of the stiffness, while the behavior for $60°$ is characterized by a monotonous stiffening. The case of fibers aligned in the direction of the stretch provides an intermediate stress.

The sensitivity analysis of the material model to the fiber material parameters are shown in Fig. 3 for uniaxial loading. The model is characterized by a marked sensitivity to the fiber stiffness K_g and to the fiber rigidity k.

Active-passive response

We consider a tissue undergoing uniaxial and biaxial stretching in the presence of a constant electric field acting in the direction 3, leading to a tetanized-like material, and apply a stretch in the direction 3 (see Fig. 4). The passive response under a constant active action is visualized in Fig. 5 for the cases $E = 10$ V/m (a,c,e) and 20 V/m (b,d,f) and for different inclination of the fibers. The figures for the uniaxial case compare with the purely passive case in Fig. 2(a). The presence of an electric field induces a contraction of the material, testified by the presence of a tensile stress at zero elastic strain. The effect is small for E=10 V/m, but it is quite relevant for $E = 20$ V/m. For the biaxial case, a non zero stress at zero elastic strain is observed also in direction 2.

(a) Uniaxial   (b) Biaxial
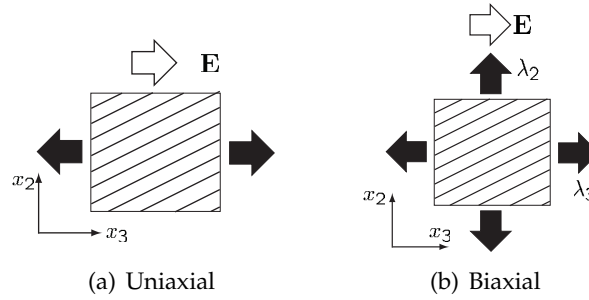
Figure 4: Schematic of the passive loading conditions for uniaxial and biaxial tests under a constant electric field E oriented in the direction 3 and imposed stretch in the direction 3. Direction 1, normal to the plane of the figure, is stress free. In uniaxial conditions, direction 2 is stress free. In biaxial conditions, the stretch ratio is $\lambda_2 / \lambda_3 = 0.75$. The fiber inclination varies between $0°$ and $90°$.

Next, we evaluate the effect of a growing electric field E acting in the direction 3, for a material confined in uniaxial and biaxial configuration, see Fig. 6. The response of the material is shown in Fig. 7 for an electric field intensity in the range $E = 10\text{-}20$ V/m. The electric field induces a stress in absence of strain. Qualitatively, in uniaxial confinement, the effect of E is equivalent to the application of a uniaxial strain. In biaxial confinement, the stress induced by a growing electric field in the two directions 3 and 2 is very different, due to the assumed dependence on the electric field direction of the inelastic strain energy density, see (4.5).

One-dimensional electromechanical problem

We conclude the set of introductory examples with the analysis of an one-dimensional problem that includes a simple phenomenological model of cardiac electrophysiology. Following [9,10], we assume that the variation in the electric potential φ –and therefore in E– is induced by the variation of ionic concentration. In particular, we refer to a simplified dimensionless three-variable (u, v, w) model of cardiac action potential generation and propagation, in the form described by [19]. The electrophysiological model introduces a normalized membrane potential u, and two transmembrane gates, a fast one, v, and a slow one, w. The dimensionless membrane potential $0 \le u \le 1$ is defined as

$$u = \frac{\varphi - V_o}{V_{\text{fi}} - V_o},$$

where φ is the electric transmembrane potential, V_o is the resting membrane potential and V_{fi} the Nernst potential of the fast inward current.

The material electric diffusion equation (2.7) in normalized form becomes

$$\frac{\partial u}{\partial t} = \frac{1}{J} \frac{\partial}{\partial X_J} \left(-J K_{IJ} \frac{\partial u}{\partial X_I} \right) + \text{I}_{\text{ion}}. \tag{4.6}$$

The total transmembrane density current I_{ion} is the sum of: (i) a slow time-independent outward current, I_{so}; (ii) a fast inward inactivation current depending on the gate v, I_{fi};
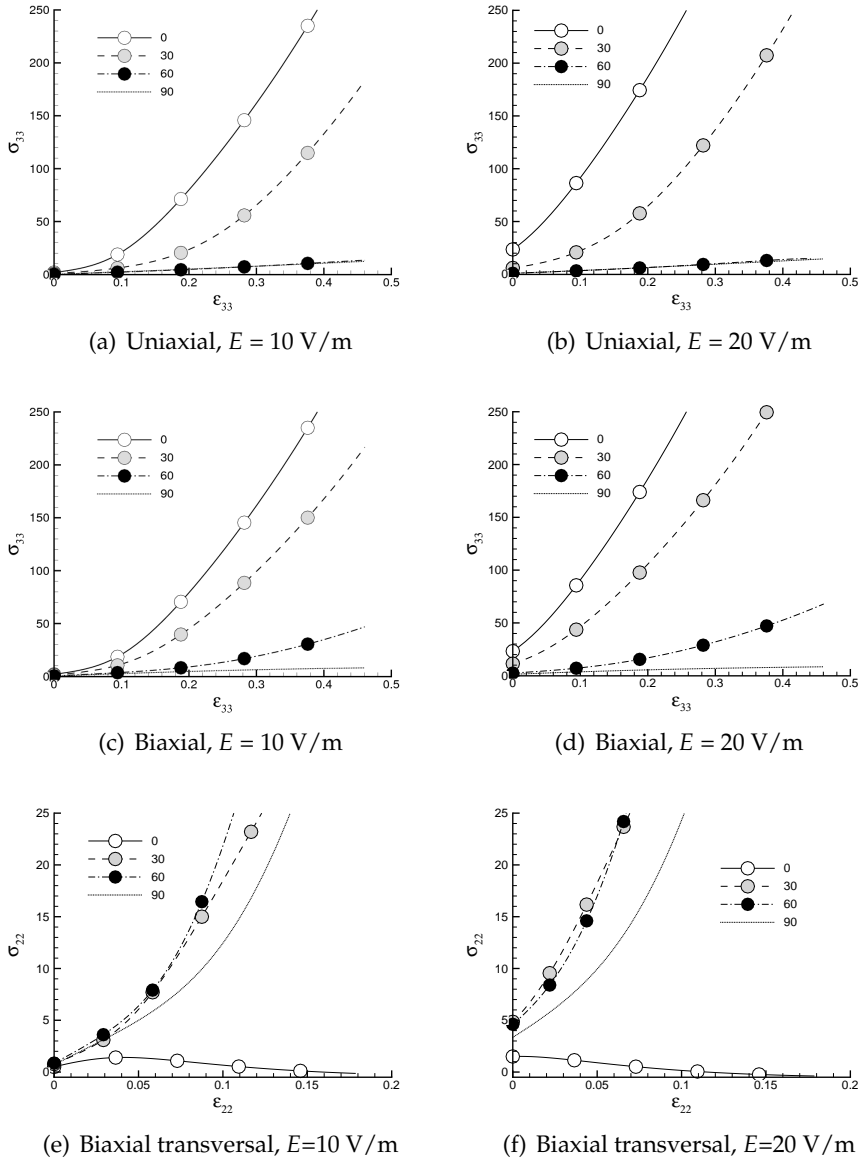
Figure 5: Uniaxial and biaxial response of the model under constant electric fields in direction 3, for different inclinations of the fibers with respect to the loading direction. Stresses in kPa.

(iii) and a slow inward inactivation current depending on the gate w, I_{si}, defined as

$$I_{so} = \frac{u}{\tau_0}\mathcal{H}(u_c - u) + \frac{1}{\tau_r}\mathcal{H}(u - u_c),$$

$$I_{fi} = -\frac{v}{\tau_d}\mathcal{H}(u - u_c)(1 - u)(u - u_c),$$

$$I_{si} = -\frac{w}{2\tau_{si}}\left(1 + \tanh\left[k_{si}\left(u - u_c^{si}\right)\right]\right),$$
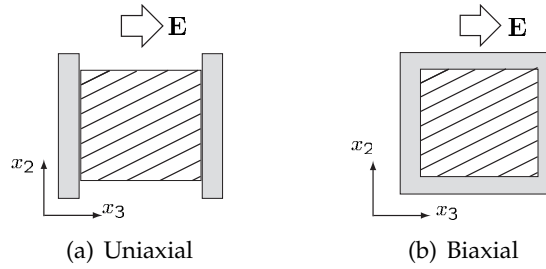
Figure 6: Schematic of the constraint for uniaxial and biaxial tests under growing electric field. Direction 1, normal to the plane of the figure, is always stress free. Direction 3 is blocked for both cases, while direction 2 is blocked for the biaxial case. The fiber inclination varies between $0°$ and $90°$.
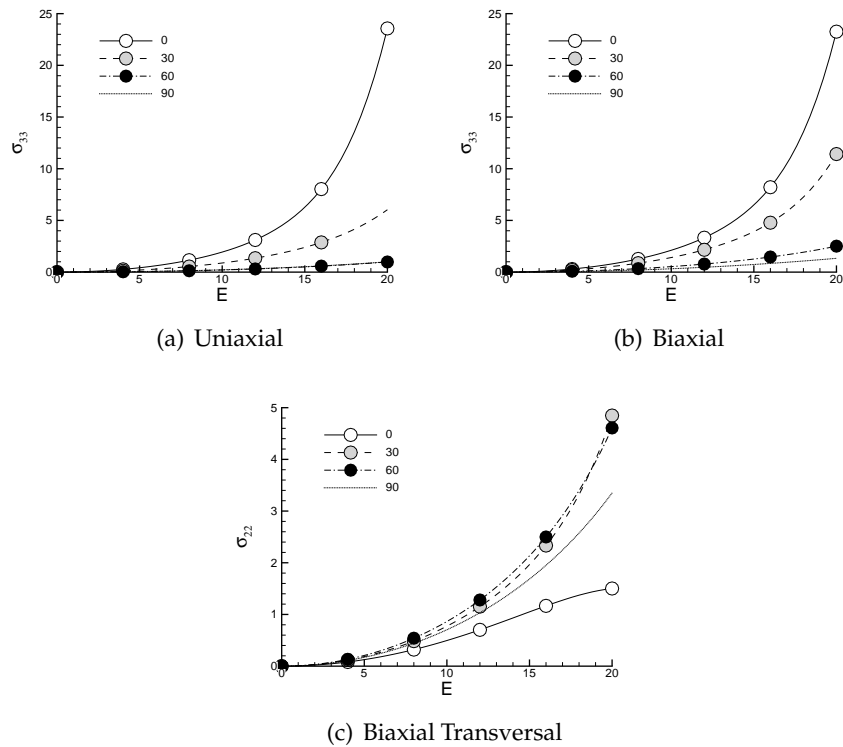
Figure 7: Mechanical response of the model constrained in uniaxial and biaxial configuration to a growing electric field in the direction 3, for different inclinations of the fibers with respect to the direction 3. Stresses in kPa, electric field in V/m.

where u_c, k_{si}, u_c^{si}, τ_d, τ_0, τ_{si} are parameters of the model and $\mathcal{H}(x)$ is the standard Heaviside step function, defined as $\mathcal{H}(x) = 0$ for $x \leq 0$ and $\mathcal{H}(x) = 1$ for $x > 0$. The variables v and w obey the equations

$$\frac{dv}{dt} = \mathcal{H}(u_c - u)\frac{(1-v)}{\tau_v^-(u)} - \mathcal{H}(u - u_c)\frac{v}{\tau_v^+}, \tag{4.7}$$

(a) Restitution curve   (b) Model dynamics
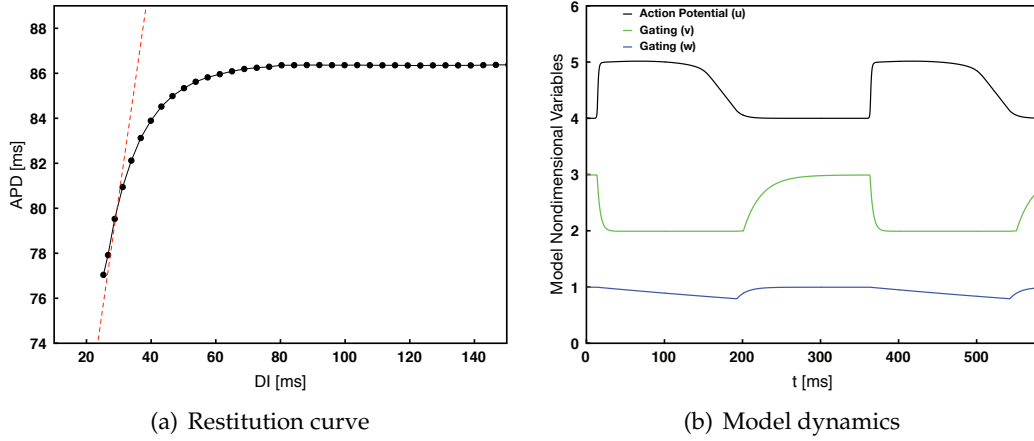
Figure 8: (a) Restitution curve built upon the 3-variable phenomenological model of cardiac action potential generation and propagation [19] according to the parametric setup fitted to a modified version of the Beeler-Reuter model [6]. The red dashed line describes the referential slope 1 of the map and the point at which the restitution curves becomes steeper than 1. (b) Zero-dimensional time course of the three model variables for two consecutive stimulations.

$$\frac{dw}{dt} = \mathcal{H}(u_c - u)\frac{(1-w)}{\tau_w^-} - \mathcal{H}(u - u_c)\frac{w}{\tau_w^+}, \tag{4.8}$$

where τ_v^+, τ_w^-, τ_w^+ are three time constants. The time constant $\tau_v^-(u)$ that governs the reactivation of the fast inward current must be defined in a different way for the two voltage ranges $u < u_v$ and $u_v < u < u_c$ as

$$\tau_v^-(u) = \mathcal{H}(u - u_v)\tau_{v1}^- + \mathcal{H}(u_v - u)\tau_{v2}^-,$$

according to the parametric setup fitted to a modified version of the Beeler-Reuter model [6], reproducing several features of the cardiac action potential [17], i.e., the conduction velocity of the transmembrane voltage, the shape and duration of the action potential signal and the restitution curves build upon constant pacing. According to the theory of one-dimensional maps, the model is able to predict the onset of arrhythmic states for fast stimulation frequencies. This states can be detected by a slope of the restitution curves greater than one [51]. To demonstrate this, in Fig. 8(a) we show the action potential duration (APD) versus the diastolic interval (DI) restitution curve obtained from the cardiac model, under constant stimulation with increasing frequency or decreasing pacing cycle length (CL). The resulting one-dimensional map reads:

$$CL = APD + DI. \tag{4.9}$$

We complete the illustration of the model by showing the time evolution of the three non-dimensional variables for two consecutive stimulations, Fig. 8(b). Noticeably, the described dynamics mimic the actual physiological transmembrane voltage (u) and the ion Na, K currents (v, w).

In the one dimensional problem, the significant direction is taken to be 3, and we exclude volumetric behaviors (e.g., $\gamma_{\text{vol}} = 0$) that cannot be considered in a uniaxial setting.

The non-zero vector and tensor components are:

$$E_3 = E, \quad a_3 = 1, \qquad F_{33} = \lambda, \quad \dot{F}_{33} = \dot{\lambda}, \qquad \lambda^i = 1 + \gamma_{\text{dev}}(E) E^2.$$

The kinematic variables and invariants reduce to

$$\lambda^e = \lambda \lambda^{i-1}, \qquad J^e = \lambda^e, \qquad I_1 = \lambda^2 + 2, \qquad I_4 = \lambda^2, \qquad \overline{I}_4^e = \lambda^{e\frac{4}{3}},$$

$$\overline{I}_1^e = \lambda^{e\frac{4}{3}} + 2\lambda^{e-\frac{2}{3}} = \lambda^{e-\frac{2}{3}} \left(\lambda^{e2} + 2 \right), \qquad \overline{I}_2^e = 2\lambda^{e\frac{2}{3}} + \lambda^{e-\frac{4}{3}} = \lambda^{e-\frac{4}{3}} \left(2\lambda^{e2} + 1 \right).$$

The Helmholtz free energy density can be rendered explicitly as

$$A(\lambda, \lambda^e, E) = \frac{1}{4} K \left(\lambda^{e2} - 1 - 2\log \lambda^e \right) + \mu_1 \left(\frac{1}{2} \lambda^{e\frac{4}{3}} + \lambda^{e-\frac{2}{3}} \right) + \mu_2 \left(\lambda^{e\frac{2}{3}} + \frac{1}{2} \lambda^{e-\frac{4}{3}} \right)$$
$$+ \frac{1}{2} \frac{K_g}{k} \left[\exp k \left(\lambda^{e\frac{4}{3}} - 1 \right)^2 - 1 \right] - \frac{1}{2} \epsilon_0 \frac{E^2}{\lambda} \left[1 + \chi + \chi^C (\lambda^2 - 1) \right],$$

where we write $\chi = \chi_{\text{iso}} + \chi_{\text{fiber}}$ and $\chi^C = \chi_{\text{iso}}^C + \chi_{\text{fiber}}^C$. The passive stress becomes

$$P_{33}^p = \left\{ \frac{1}{2} K \left(\lambda^{e2} - 1 \right) + \frac{2}{3} \mu_1 \lambda^{e-\frac{2}{3}} \left(\lambda^{e2} - 1 \right) + \frac{2}{3} \mu_2 \lambda^{e-\frac{4}{3}} \left(\lambda^{e2} - 1 \right) \right.$$
$$\left. + \frac{4}{3} \lambda^{e\frac{4}{3}} \left(\lambda^{e\frac{4}{3}} - 1 \right) K_g \exp k \left(\lambda^{e\frac{4}{3}} - 1 \right)^2 \right\} \frac{1}{\lambda},$$

and the active stress is

$$P_{33}^a = \frac{1}{2} \epsilon_0 \left[1 + \chi - \chi^C (1 + \lambda^2) \right] \frac{E^2}{\lambda^2}.$$

Note that the term

$$\epsilon_r(\lambda) = 1 + \chi - \chi^C (1 + \lambda^2)$$

defines the relative dielectric permittivity $\epsilon_r(\lambda)$ of the materials a function of the stretch. The passive tangent stiffness is

$$C_{3333}^p = \left\{ \frac{1}{2} K \left(\lambda^{e2} + 1 \right) + \frac{2}{9} \mu_1 \lambda^{e-\frac{2}{3}} \left(\lambda^{e2} + 5 \right) - \frac{2}{9} \mu_2 \lambda^{e-\frac{4}{3}} \left(\lambda^{e2} - 7 \right) \right.$$
$$\left. + \frac{4}{9} \lambda^{e\frac{4}{3}} \left[8k \left(\lambda^{e2} - \lambda^{e\frac{2}{3}} \right)^2 + 5\lambda^{e\frac{4}{3}} - 1 \right] K_g \exp k \left(\lambda^{e\frac{4}{3}} - 1 \right)^2 \right\} \frac{1}{\lambda^2},$$

and the active tangent stiffness is

$$C_{3333}^a = -\epsilon_0 \left(1 + \chi - \chi^C \right) \frac{E^2}{\lambda^3}.$$

Table 2: Parameters of the electrophysiological model used in the uniaxial example of application [19]. The diffusion tensor K_{IJ} in (4.6) equals k_0 in the fiber direction and $0.2k_0$ in the two directions orthogonal to the fibers.

V_{fi}	V_0	u_c	u_v	u_v^{si}	k_{si}	k_0	τ_d
[mV]	[mV]	-	-	-	-	[cm^2/ms]	[μ F/cm^2]
85	15	0.13	0.055	0.85	8	10^{-3}	0.25

τ_r	τ_{si}	τ_0	τ_v^+	τ_{v1}^-	τ_{v2}^-	τ_w^+	τ_w^-
[ms]	[ms]	[ms]	[ms]	[ms]	[ms]	[ms]	[ms]
50	45	8.3	3.33	1000	19.6	6.67	11

The electric diffusion equation becomes

$$C_E(\lambda)\frac{\partial \varphi}{\partial t} = \frac{\partial}{\partial X}\left(\frac{1}{\lambda}k_E\frac{\partial \varphi}{\partial X}\right) + I_E(\lambda).$$

We integrated the material constants reported in Table 1 with the electrophysiological parameters taken from [19], see Table 2.

We consider a one-dimensional system 100 mm in length. The domain is discretized in 240 finite elements of uniform size, adopting a different order for the mechanical and the electrophysiology problem, for a total of 2404 degrees of freedom. The scalar displacement field is discretized by means of fourth order polynomial elements (961 displacement degrees of freedom). The three scalar fields u, v, and w governing the electrophysiological problem, see Eqs. (4.6)-(4.8), are discretized by means of second order polynomial elements (481 degrees of freedom for each variable), leading to a linear electric field in each element. The extracellular medium has been treated as vacuum, with no additional electric field. For the electrophysiological problem we impose homogeneous Neumann boundary conditions, while, in order to recover the 20% physiological deformation of the tissue, Robin spring-like mechanical boundaries are adopted.

We solve the fully coupled electromechanical problem with a monolithic approach, adopting a direct time-dependent numerical scheme based on backward differential formulae, with relative tolerance $\epsilon_{\text{tol}} = 10^{-5}$ and absolute tolerance $\epsilon = 10^{-6}$ on the whole problem.

At mid-point of the one-dimensional domain we apply a square wave stimulation current, with decreasing pacing intervals, i.e., 150, 125, 100, 90, 80, 70, 60, 50 ms, in line with standard restitution protocols used in cardiac dynamics [18, 21]. The stimulus generates two symmetric action potential waves propagating in opposite direction towards the boundaries. An observation point is located at 5 mm from the left boundary.

Fig. 9(a) shows the time history of the action potential at the observation point. The action potential varies within the physiological range [-80, 20] mV. Fig. 9(b) shows the shape of the electric field generated by the membrane voltage, with intensity in the range [-20, 60] V/m. The inelastic strain signal produced by the electromechanical coupling is

(a) Voltage membrane

(b) Electric Field

(c) Inelastic stretch

(d) Cauchy stress
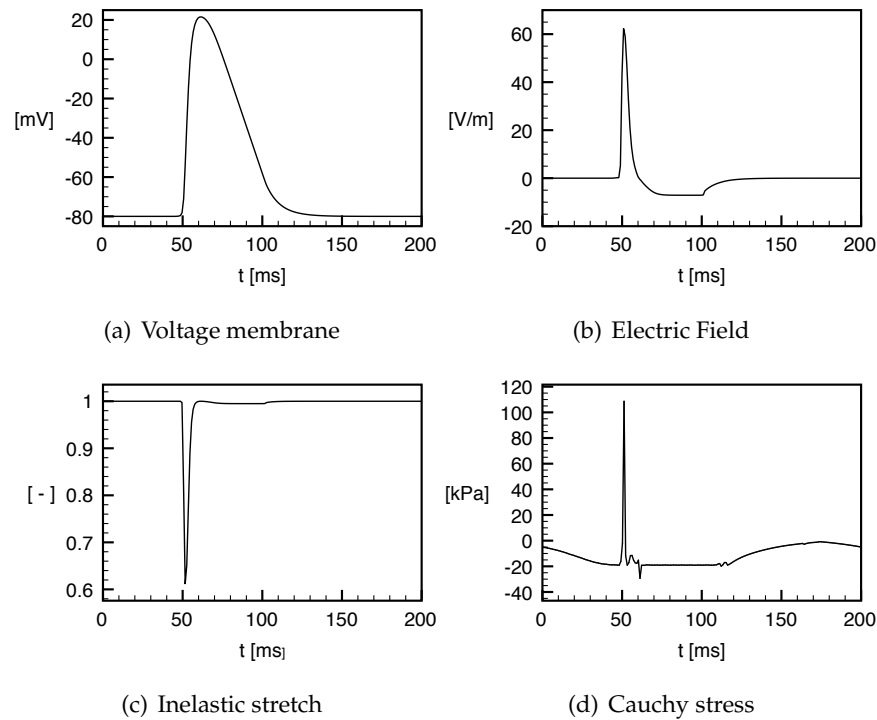
Figure 9: Numerical point signals diagrams characterizing the one-dimensional fully coupled electromechanical problem. The observation point is located 5 mm far from the left boundary. (a) Voltage membrane, (b) electric field, (c) inelastic stretch λ^a, (d) total Cauchy stress.

visualized in Fig. 9(c). The maximum active contraction reaches roughly the 40% of the original length. The total stress signal is reported in Fig. 9(d), and is characterized by a 100 kPa tensile peak. Note that the tensile stress peak covers a narrow region of the domain, whereas the stress field is very limited everywhere else. The four diagrams are in phase, as expected in a purely elastic material with no viscosity and no dissipation.

Fig. 10 shows the space-time diagrams of the membrane voltage, electric field intensity, inelastic strain and total Cauchy stress for the one-dimensional simulation. Clearly the model is able to reproduce a stress signal consistent with the voltage signal. Additionally, we observe that the four signals propagate at an average speed of 0.4 m/s. Small deviations from the average velocity, testified by the non straight path of the spatiotemporal plots, are due to the electromechanical feedback of the model.

The effects of elasticity on the electric field are demonstrated through Figs. 11 and 12, where we compare the numerical results of a rigid and of a deformable material. We consider a signal applied to the left boundary of the one dimensional domain, and refer to five observation points located at 1, 2, 3, 4 and 5 cm, respectively, from the signal source. The nonlinear coupling between electricity and elasticity is responsible of the differences between the two analyses. In particular, we highlight: (i) the differences in the repolar-

(a) Voltage membrane

(b) Electric field

(c) Inelastic stretch

(d) Cauchy stress
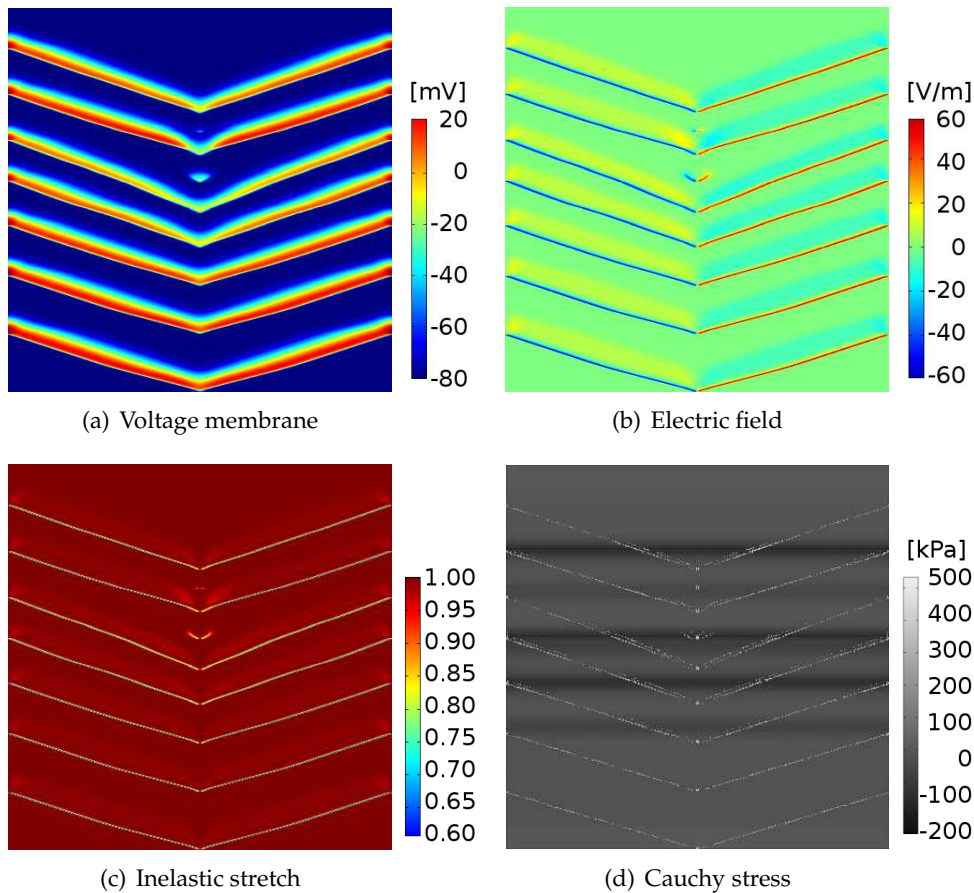
Figure 10: Space-time diagrams obtained from numerical simulations of the fully coupled electromechanical problem. The pacing signal is originated at the center of the domain. Space domain (0-100 mm) in the horizontal axis. Time (0-1000 ms) in the vertical axis. (a) Voltage membrane, (b) electric field, (c) inelastic stretch λ^a, (d) total Cauchy stress.

ization times, which lead to different color maps of the electric field, see Figs. 11(b,c); (ii) the deviation and deceleration of the conduction velocity in the deformable case, denounced by the wider space-time stripes with a reduced average slope. The trend is also visualized by the five point diagrams in Fig. 12 and is in agreement with previous results [8]; (iii) the reduction of the electric field intensity in the elastic case with respect to the rigid one, even for equal amplitudes of the membrane potential, see Fig. 12. The observed effects are mainly due to the nonlinear feedback that elasticity creates in the electric problem, due to the presence of the elastic terms in the diffusive contribution of the voltage propagation equation, see Eqs. (2.6)-(2.7). Such phenomena are typical of active biological media and characterize the natural disposition of the tissue to generate refractoriness gradients, which play an important role in the complex dynamics of two- and three-dimensional models [20].

(a) Rigid voltage membrane

(b) Rigid electric field

(c) Deformed voltage membrane

(d) Deformed electric field
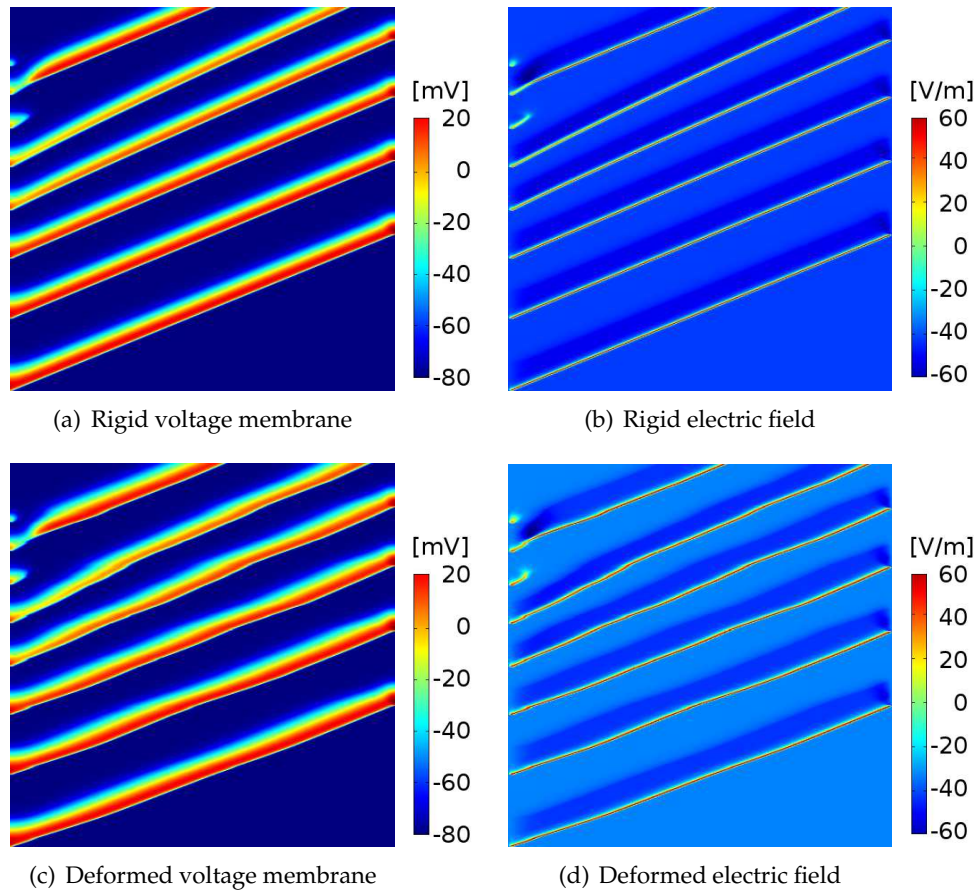
Figure 11: Numerical space-time diagrams: (a,b) purely electric problem (or rigid case); (c,d) fully coupled electromechanical problem (or deformed case). The pacing signal is located at the left end of the domain. Space domain (0-100 mm) in the horizontal axis. Time (0-800 ms) in the vertical axis.

5 Conclusions

We presented a thermodynamically consistent electromechanical approach to the definition of material models able to describe the behavior of active materials. The main motivation of our study was an attempt to propose a solution to the dilemma that afflicts many scientists aiming at modeling the behavior of active tissues, in particular bio-tissues such as muscles and heart. The most consolidated approaches are based on the concept of active stress. Although the introduction of the active stress component encompasses the key aspects related to the description of the subcellular electrophysiological dynamics of the tissue, it is rather difficult to justify the presence of active stresses from the thermodynamical point of view. On the other side, the decomposition of a generic deformation into elastic and inelastic part is very familiar to mechanicians, either in terms of additive decomposition (used mostly in linearized kinematics) or in terms of multiplicative
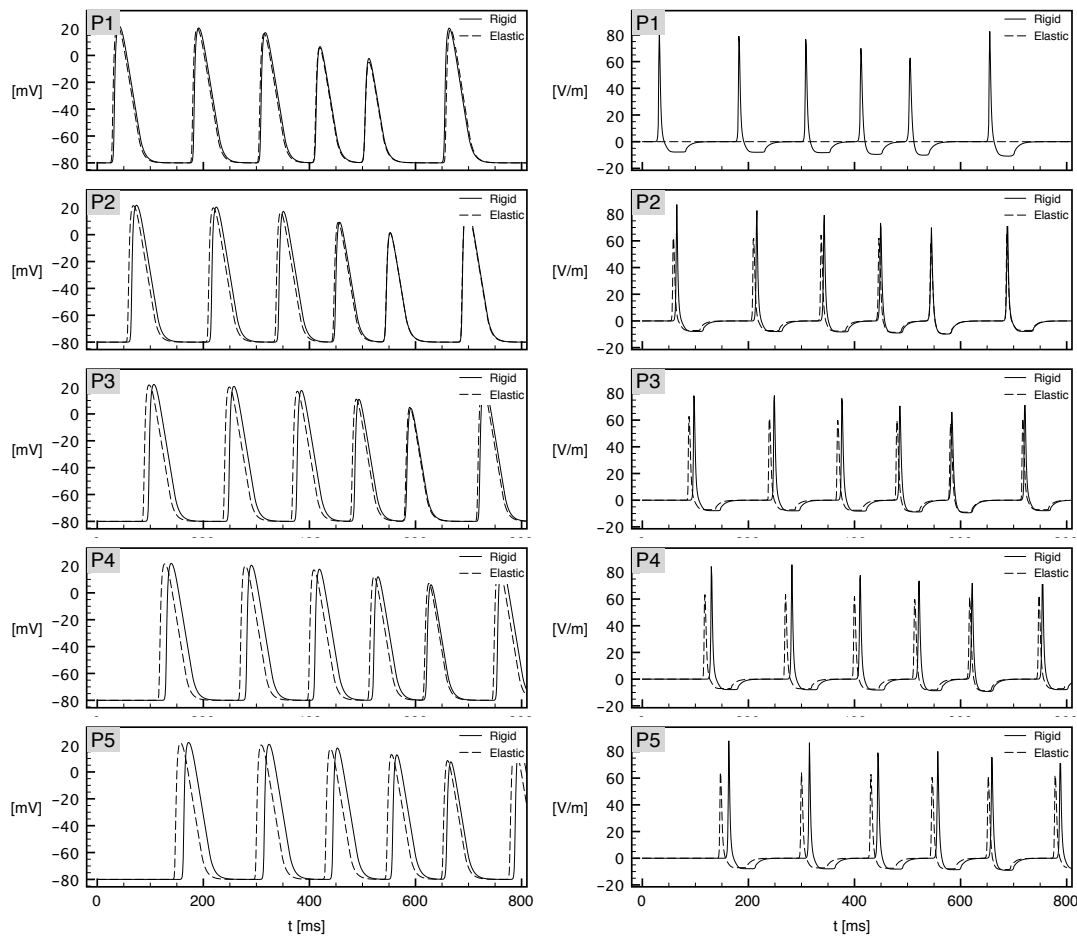
Figure 12: Point signals diagrams with voltage membrane (left) and electric field (right). Comparison between the purely electric case (solid line) and the electromechanical case (dashed line). The five diagrams refer to the five spatial locations at 1, 2, 3, 4 and 5 cm from the signal source on the left side of the one-dimensional domain. Times in the horizonal axis are in ms.

decomposition (used in finite kinematics). In dealing with active materials, it is spontaneous to think of the existence of an inelastic deformation that may carry the effect of microstructural changes of the material, or the effect of coupled fields (such as electrical, chemical, magnetic, and others). Often in the literature such deformations are referred to as eigendeformations; in the mechanics of active tissues they are called instead active deformations.

In the present study, we proposed a new point of view that conciliate the concepts of active stress and active strain through the definition of a suitable expression of the Helmholtz strain energy density. We propose to combine the multiplicative decomposition in elastic and inelastic parts of the deformation gradient with the additive decomposition of the strain energy. The strain energy is conceived as the sum of two terms,

one purely elastic, dependent on the elastic deformation gradient only; and the other dependent on other non-mechanical fields and on the total deformation gradient. The expression of the strain energy density can be chosen according to the particular applications that one has in mind. In the present study, we focus on fiber reinforced tissues, that describe the typical structure of muscle and heart myocytes. By the way of example, we played with a simple model that accounts for the presence of a single set of strongly aligned fibers, and the consequent anisotropy of the material is accounted for by means of standard structure tensors.

Since we disregarded thermal effects, viscosity and any other source of dissipation, the simple model adopted here is characterized by a reduced number of material constant: nine, five for the mechanical behavior and four for the electromechanical coupling. Simple tests showing the pure passive and the combined active/passive response of the model under uniaxial and biaxial loading proved that the coupling is nicely captured by the model. In our original plans, we had in mind to develop a model able to include the electrophysiology of the heart. The one-dimensional example shown here, that includes a simplified yet realistic model of cardiac electrophysiology (sixteen constants), demonstrates that the activation through a periodic electric current induces an active strain wave, and by compatibility, elastic strain and equilibrium stress waves. Upon a suitable calibration of the material parameters, the mechanical model is able to reproduce the experimental evidence of cardiac tissue deformations up to 20%, as it can be seen in Figs. 9(c) and 10(c), where the inelastic stretch distribution in time and space, respectively, are reported.

Future extensions of this work include the development of solid models of fiber reinforced soft tissues considering fibers recruitment activation [23], and simplified models of the muscle and of the heart, where we will apply the fully three-dimensional material model. We believe that the use of a thermodynamically consistent material model in biological tissues will provide a valid support to a better understanding of pathological conditions and their treatment. For example, in order to treat with optimal efficiency arrhythmic events in the myocardium, low energy defibrillating procedures are being developed. Regrettably, most procedures are modeled through purely electric models [42], although it has been proved that elasticity introduces marked differences in the quantitative response of simplified models [8,61]. Moreover, complex spatio-temporal cardiac arrhythmias could be explored in terms of electromechanics rather than in terms of electric alternans. In particular, the intra- and extra-cellular calcium dynamics, strongly related to the excitation-contraction mechanisms, would benefit of a fully coupled approach enhancing the role of bi-domain structure and subcellular reactions, in view of a multiscale theoretical formulation.

Further extensions will account for the treatment of viscous behaviors, similar to the ones observed in active biological tissues [7]; for a more realistic description of the anisotropy by considering dispersion of the fiber orientation [72,73]; and for thermal diffusion. It is well known that active electromechanical systems such as heart and intestine are very sensitive to thermal variations [18,20,22]. The latter extension will allow to eval-

uate quantitatively the effects of thermal cooling and heating, fundamental in analyzing pathological conditions and the treatment of diseases.

Acknowledgments

Appendix A

The following expressions hold for the particular choice of strain energy function, see Eqs. (4.1)-(4.3).

Passive stress

$$P_{iJ}^p = \left[\frac{1}{2} K \left(J^{e\,2} - 1 \right) F_{Hi}^{e\,-1} + F_{iK}^e S_{\mathrm{dev}\,KH}^e \right] F_{HJ}^{i\,-1},$$

$$S_{\mathrm{dev}\,KH}^e = J^{e-2/3} \left(\delta_{KL}\delta_{HM} - \frac{2}{3} C_{KH}^{e\,-1} C_{LM}^e \right) \overline{S}_{LM}^e,$$

$$\overline{S}_{LM}^e = \frac{1}{2} \left(\mu_1 + \mu_2 \overline{I}_1^e \right) \delta_{LM} - \frac{1}{2} \mu_2 \overline{C}_{LM}^e + K_g \left(\overline{I}_4^e - 1 \right) \exp k \left(\overline{I}_4^e - 1 \right)^2 n_L n_M.$$

Active stress

$$P_{rS}^a = \epsilon_0 J E_I F_{Im}^{-1} \left\{ \left(\delta_{mr} F_{Si}^{-1} - \frac{1}{2} \delta_{mi} F_{Sr}^{-1} \right) \left[\left(1 + \chi_{\mathrm{iso}} + \chi_{\mathrm{iso}}^C (I_1 - 1) \right) \delta_{ij} \right. \right.$$
$$\left. \left. + \left(\chi_{\mathrm{fiber}} + \chi_{\mathrm{fiber}}^C (I_4 - 1) \right) n_i n_j \right] - \delta_{mi} F_{rH} \left[\chi_{\mathrm{iso}}^C \delta_{HS} \delta_{ij} + \chi_{\mathrm{fiber}}^C n_H n_S n_i n_j \right] \right\} F_{Kj}^{-1} E_K.$$

References

[1] R. R. Aliev and A. V. Panfilov. A simple two-variable model of cardiac excitation. Chaos Solitons Fractals, 7(3):293–301, 1996.

[2] D. G. Allen and J. C. Kentish. The cellular basis of the length-tension relation in cardiac muscle. Journal of Molecular and Cellular Cardiology, 17:821–840, 1985.

[3] D. Ambrosi, G. Arioli, F. Nobile, and A. Quarteroni. Electromechanical coupling in cardiac dynamics: The active strain approach. SIAM Journal of Applied Mathematics, 71(2):605–621, 2011.

[4] A. Ask, A. Menzel, and M. Ristinmaa. Electrostriction in electro-viscoelastic polymers. Mechanics of Materials, 50:9–21, 2012.

[5] A. Ask, A. Menzel, and M. Ristinmaa. Phenomenological modeling of viscous electrostrictive polymers. International Journal of Non-Linear Mechanics, 47:156–165, 2012.

[6] G. W. Beeler and H. Reuter. Reconstruction of the action potential of ventricular myocardial fibres. Journal of Physiology, 268:177–210, 1977.

[7] D. Bini, C. Cherubini, and S. Filippi. Viscoelastic FitzHugh-Nagumo models. Physical Review E, 72:041929, 2005.

[8] C. Cherubini, S. Filippi, and A. Gizzi. Electroelastic unpinning of rotating vortices in biological excitable media. Physical Review E, 85:031915, 2012.

[9] C. Cherubini, S. Filippi, P. Nardinocchi, and L. Teresi. An electromechanical model of cardiac tissue: Constitutive issues and electrophysiological effects. Progress in Biophysics & Molecular Biology, 97:562–573, 2008.

[10] C. Cherubini, S. Filippi, P. Nardinocchi, and L. Teresi. Electromechanical modelling of cardiac tissue. In A. Kamin and I. Kiseleva, editors, Mechanosensitivity of the Heart. Vol. 3, pages 421–449. Springer, Berlin, 2010.

[11] B. D. Coleman and W. Noll. The thermodynamics of elastic materials with heat conduction and viscosity. Archives of Rational Mechanics and Analysis, 13(1):167–178, 1963.

[12] S. Dokos, B. H. Smaill, A. A Young, and I. J. LeGrice. Shear properties of passive ventricular myocardium. American Journal of Physiological and Heart Circulatory Physiology, 283:H2650–2659, 2002.

[13] A. Dorfmann and R. W. Ogden. Nonlinear electroelasticity. Acta Mechanica, 174:167–183, 2005.

[14] C. Eckart. The thermodynamics of irreversible processes, IV. The theory of elasticity and anelasticity. Physical Reviews, 73:373–380, 1948.

[15] D. A. Eisner, H. S. Choi, M. E. Diaz, S. C. O'Neill, and A. W. Trafford. Integrative analysis of calcium cycling in cardiac muscle. Circulation Research, 87:1087–1094, 2000.

[16] A. C. Eringen and G. A. Maugin. Elastodynamics of Continua. Foundations and Solid Media. Spinger-Verlag, New York, 1990.

[17] F. H. Fenton and E. M. Cherry. Models of cardiac cell. Scholarpedia, 3:1868, 2008.

[18] F. H. Fenton, A. Gizzi, C. Cherubini, and S. Filippi. Role of temperature on nonlinear cardiac dynamics. Physical Review E, 87:042717, 2013.

[19] F. H. Fenton and A. Karma. Vortex dynamics in three-dimensional continuous myocardium with fiber rotation: Filament instability and fibrillation. Chaos, 8:1054, 1998.

[20] S. Filippi, A. Gizzi, C. Cherubini, S. Luther, and F. H. Fenton. Mechanistic insights into hypothermic ventricular fibrillation: the role of temperature and tissue size. Europace, 16:424–434, 2014.

[21] A. Gizzi, E. M. Cherry, Gilmour R. F. Jr, S. Luther, S. Filippi, and F. H. Fenton. Effects of pacing site and stimulation history on alternans dynamics and the development of complex spatiotemporal patterns in cardiac tissue. Frontiers in Physiology, 4:71, 2013.

[22] A. Gizzi, C. Cherubini, S. Migliori, R. Alloni, R. Portuesi, and S. Filippi. On the electrical intestine turbulence induced by temperature changes. Physical Byology, 7:016011, 2010.

[23] A. Gizzi, M. Vasta, and A. Pandolfi. Modeling collagen recruitment in hyperelastic biomaterial models with statistical distribution of the fiber orientation. International Journal of Engineering Science, 78:48–60, 2014.

[24] S. Goktepe, S. N. S. Acharya, J. Wong, and E. Kuhl. Computational modeling of passive myocardium. International Journal for Numerical Methods in Biomedical Engineering, 27(1):1–12, 2011.

[25] S. Göktepe, A. Menzel, and E. Kuhl. Micro-structurally based kinematic approaches to elec-

tromechanics of the heart. In Computer Models in Biomechanics, pages 175–187. Springer Netherlands, 2013.

[26] H. L. Granzier and T. C Irving. Passive tension in cardiac muscle: contribution of collagen, titin, microtubules, and intermediate filaments. Biophysical Journal, 68:1027–1044, 1995.

[27] J. M. Guccione, A. D. McCulloch, and L. K. Waldman. Passive material properties of intact ventricular miocardium determined from a cylindrical model. Journal of Biomechanical Engineering, 113(1):42–55, 1991.

[28] Z. Guo, F. Caner, X. Peng, and B. Moran. On constitutive modelling of porous neo-Hookean composites. Journal of the Mechanics and Physics of Solids, 56:2338–2357, 2008.

[29] Z. Y. Guo, X. Q. Peng, and B. Moran. A composites-based hyperelastic constitutive model for soft tissue with application to the human annulus fibrosus. Journal of the Mechanics and Physics of Solids, 68:1027–1044, 2006.

[30] A. V. Hill. The heat of shortening and dynamics constants of muscles. Proceedings of the Royal Society of London, B, 367(843):136–195, 1938.

[31] G. A. Holzapfel and R. W. Ogden. Constitutive modelling of passive myocardium: A structurally based framework for material characterization. Phylosophycal Transactions of the Royal Society, A, 367:3445–3475, 2009.

[32] P. J. Hunter, M. P. Nash, and G. B. Sands. Computational Electromechanics of the Heart. Wiley, London, 1997.

[33] K. Hutter, A.F.A. Ven, and A. Ursescu. Electromagnetic Field Matter Interactions in Thermoelastic Solids and Viscous Fluids. Lecture Notes in Physics. Springer, 2006.

[34] M. Itskov, A. E. Ehret, and D. Mavrilas. A polyconvex anisotropic strain-energy function for soft collagenous tissues. Biomechanics and Modeling in Mechanobiology, 5(1):17–26, 2006.

[35] R. H. Keldermann, M. P. Nash, and A. V. Panfilov. Modeling cardiac mechano-electrical feedback using reaction-diffusion-mechanics systems. Physica D, 238:1000–1007, 2009.

[36] C. Kittel. Introduction to Solid State Physics. John Wiley & Sons, New York, 2004.

[37] L. D. Landau, E. M. Lifshitz, and L. P. Pitaevskii. Electrodynamics of Continuous Media, volume 8. Butterworth-Heinemann, Oxford, 1984.

[38] E. H. Lee. Elastic-plastic deformation at finite strains. ASME, Journal of Applied Mechanics, 36:1–6, 1969.

[39] I. J. LeGrice, P. J. Hunter, and B. H. Smaill. Laminar structure of the heart: A mathematical model. American Journal of Physiology - Heart Circulation Physiology, 272:H2466–H2476, 1997.

[40] V. A. Lubarda. Constitutive theories based on the multiplicative decomposition of deformation gradient: Thermoelasticity, elastoplasticity, and biomechanics. Applied Mechanics Reviews, 57(2):95–108, 2004.

[41] J. Lubliner. On the thermodynamic foundations of nonlinear solid mechanics. International Journal of Non-Linear Mechanics, 7:237–254, 1972.

[42] S. Luther, F. H. Fenton, B. G. Kornreich, A. Squires, P. Bitthn, D. Hornung, M. Zabel, J. Flanders, A. Gladuli, L. Campoy, E. M. Cherry, G. Luther, G. Hasenfuss, V. I. Krinsky, A. Pumir, Gilmour R. F. Jr, and Bodenschatz. Low-energy control of electrical turbulence in the heart. Nature Letter, 475(235–239):1000–1007, 2011.

[43] G. A. Maugin. Continuum Mechanics of Electromagnetic Solids. North-Holland Series in Applied Mathematics and Mechanics, volume 33. Elsevier Science, Amsterdam, 1988.

[44] R. M. McMeeking and C. M. Landis. Electrostatic forces and stored energy for deformable dielectric materials. Journal of Applied Mechanics, 72:581–590, 2005.

[45] R. M. McMeeking, C. M. Landis, and M. A. Jimenez. A principle of virtual work for com-

bined electrostatic and mechanical loading of materials. International Journal of Non-Linear Mechanics, 42:831–838, 2007.

[46] C. Miehe, B. Kiefer, and D. Rosato. An incremental variational formulation of dissipative magnetostriction at the macroscopic continuum level. International Journal of Solids and Structures, 48:1846–1866, 2011.

[47] A. Montanaro. On the constitutive relations for second sound in thermo-electroelasticity. Archives of Mechanics, 63(3):225–254, 2011.

[48] P. Nardinocchi and L. Teresi. On the active response of soft living tissues. Journal of Elasticity, 88:27–39, 2007.

[49] M. P. Nash and A. V. Panfilov. Electromechanical model of excitable tissue to study reentrant cardiac arrythmias. Progress in Biophysics & Molecular Biology, 85:501–522, 2004.

[50] A. A. Niederer, H. E. D. J. ter Keurs, and N. P. Smith. Modelling and measuring electromechanical coupling in the rat heart. Experimental Physiology, 94(5):529–540, 2009.

[51] J. B. Nolasco and R. W. Dahlen. A graphic method for the study of alternation in cardiac action potentials. Journal of Applied Physiology, 2:191–196, 1968.

[52] G. M. Odegard, T. L. Haut Donahue, D. A. Morrow, and K. R. Kaufman. Constitutive modelling of skeletal muscle tissue with an explicit strain-energy function. Journal of Biomechanical Engineering, 130:061017, 2008.

[53] R. W. Ogden and D. Steigman. Mechanics and Electrodynamics of Magneto- and Electroelastic Materials. CISM International Centre for Mechanical Sciences, Springer, Udine, 2011.

[54] M. Ortiz and A. Pandolfi. A variational cam-clay theory of plasticity. Computer Methods in Applied Mechanics and Engineering, 193:2645–2666, 2004.

[55] M. Ortiz and L. Stainier. The variational formulation of viscoplastic constitutive updates. Computer Methods in Applied Mechanics and Engineering, 171:419–444, 1999.

[56] A. Pandolfi, S. Conti, and M. Ortiz. A recursive-faulting model of distributed damage in confined brittle materials. Journal of the Mechanics and Physics of Solids, 54:1972–2003, 2006.

[57] A. V. Panfilov, R. H. Keldermann, and M. P. Nash. Self-organized pacemakers in a coupled reaction-diffusion-mechanics system. Physical Review Letters, 95:258104, 2005.

[58] Y.-H. Pao and K. Hutter. A dynamic theory for magnetizable elastic solids with thermal and electrical conduction. Journal of Elasticity, 2:89–114, 1974.

[59] P. E. Paulev and G. C. Zubieta. Textbook in Medical Physiology and Pathophysiology Essentials and Clinical Problems. Copenhagen, Denmark, 2000.

[60] P. Podio-Guidugli. A virtual power format for thermomechanics. Continuum Mechanics and Thermodynamics, 20:479–487, 2009.

[61] A. Pumir, S. Sinha, S. Sridhar, M. Argentina, M. Hörning, S. Filippi, C. Cherubini, S. Luther, and V.I. Krinsky. Wave-train-induced termination of weakly anchored vortices in excitable media. Physical Review E, 81:010901, 2010.

[62] A. W. Richards and G. M. Odegard. Constitutive modelling of electrostrictive polymers using a hyperelasticity-based approach. Journal of Applied Mechanics, 77:014502, 2010.

[63] E. K. Rodrigez, A. Hoger, and A. D. McCulloch. Stress-dependent finite growth in soft elastic tissues. Journal of Biomechanics, 27:455–467, 1994.

[64] J. M. Rogers and A. D. McCulloch. A collocation-Galerkin finite element model of cardiac action potential propagation. IEEE Transactions of Biomedical Engineering, 41:743–757, 1994.

[65] R. Ruiz-Baier, A. Gizzi, S. Rossi, C. Cherubini, A. Laadhari, S. Filippi, and A. Quarteroni. Mathematical modeling of active contraction in isolated cardiomyocytes. Mathematical Methods in Biology, doi: 10.1093/imammb/dqt009, 2013.

[66] H. Schmid, Y. K. Wang, J. Ashton, A. E. Ehret, S. B. S. Krittian, M. P. Nash, and P. J. Hunter. Myocardial material parameter estimation: A comparison of invariant based orthotropic constitutive equations. Computer Methods in Biomechanics and Biomedical Engineering, 12:283–295, 2009.

[67] J. C. Simo. A framework for finite strain elastoplasticity based on maximum plastic dissipation and the multiplicative decomposition: Part I. Continuum formulation. Computer Methods in Applied Mechanics and Engineering, 66:199–219, 1988.

[68] A. J. M. Spencer. Deformations of fibre-reinforced materials. Oxford Science Research Papers, Oxford, 1972.

[69] R. Stojanovic, S. Djuric, and L. Vujosevic. On finite thermal deformations. Archives of Mechanics Stosow, 16:103–108, 1964.

[70] Z. Suo. Theory of dielectric elastomers. Acta Mechanica Solida Sinica, 23(6):549–578, 2010.

[71] Z. Suo, X. Zhao, and W. H. Greene. A nonlinear field theory of deformable dielectrics. Journal of the Mechanics and Physics of Solids, 56:467–486, 2008.

[72] M. Vasta, A. Gizzi, and A. Pandolfi. On three- and two-dimensional fibers distributed models of biological tissues. Probabilistic Engineering Mechanics, In Press. DOI: 10.1016/j.probengmech.2014.05.003

[73] M. Vasta, A. Pandolfi, and A. Gizzi. A fiber distributed model of biological tissues. Procedia IUTAM, 6:79–86, 2013.

[74] F. Vogel, R. Bustamante, and P. Steinmann. On some mixed variational principles in electro-elastostatics. International Journal of Non-Linear Mechanics, 47:341–354, 2012.

[75] D. K. Vu and P. Steinmann. On 3-D coupled BEM–FEM simulation of nonlinear electro-elastostatics. Computer Methods in Applied Mechanics and Engineering, 201–204:82–90, 2012.

[76] D. K. Vu and P. Steinmann. On the spatial and material motion problems in nonlinear electro-elastostatics with consideration of free space. Mathematics and Mechanics of Solids, 10.1177/1081286511430161, 2012.

[77] Q. Yang, L. Stainier, and M. Ortiz. A variational formulation of the coupled thermo-mechanical boundary-value problem for general dissipative solids. Journal of the Mechanics and Physics of Solids, 54:401–424, 2006.

[78] M. A. Zulliger, A. Rachev, and N. Stergiopulos. A constitutive formulation of arterial mechanics including vascular smooth muscle tone. American Journal of Physiology - Heart Circulation Physiology, 287:H1335–H1343, 2004.